DOKUZ EYLÜL UNIVERSITY
GRADUATE SCHOOL OF NATURAL AND APPLIED SCIENCES

DESIGN AND IMPLEMENTATION OF A LIGHTWEIGHT AND MODULAR BIPED ROBOT FOR HUMAN-LIKE LOCOMOTION

by
Tolga OLCAY

October, 2016
İZMİR

DESIGN AND IMPLEMENTATION OF A LIGHTWEIGHT AND MODULAR BIPED ROBOT FOR HUMAN-LIKE LOCOMOTION

A Thesis Submitted to the
Graduate School of Natural and Applied Sciences of Dokuz Eylül University
In Partial Fulfillment of the Requirements for the Degree of Doctor of Philosophy in Mechatronics Engineering

by
Tolga OLCAY

October, 2016
İZMİR

Ph.D THESIS EXAMINATION RESULT FORM

We have read the thesis entitled **"DESIGN AND IMPLEMENTATION OF A LIGHTWEIGHT AND MODULAR BIPED ROBOT FOR HUMAN-LIKE LOCOMOTION"** completed by **TOLGA OLCAY** under supervision of **ASST. PROF. DR. AHMET ÖZKURT** and we certify that in our opinion it is fully adequate, in scope and in quality, as a thesis for the degree of Doctor of Philosophy.

Asst. Prof. Dr. Ahmet ÖZKURT

Supervisor

Prof. Dr. Zeki KIRAL

Thesis Committee Member

Assoc. Prof. Dr. M. Evren TOYGAR

Thesis Committee Member

Prof. Dr. Şeniz Ertuğrul

Examining Committee Member

Prof. Dr. Aydoğan Savran

Examining Committee Member

Prof.Dr. Emine İlknur CÖCEN
Director
Graduate School of Natural and Applied Sciences

ACKNOWLEDGMENTS

I would like to thank to my advisor Asst. Prof. Dr. Ahmet ÖZKURT because of suggestions, helps and supports for the research and writing of this thesis. I also want to thank to Asst. Prof. Dr. Taner AKKAN because of their help and encouragements.

Finally, thanks for her helps, patience and love my wife Çiğdem and my daughter Öykü, and for all supports my father and mother.

Tolga OLCAY

DESIGN AND IMPLEMENTATION OF A LIGHTWEIGHT AND MODULAR BIPED ROBOT FOR HUMAN-LIKE LOCOMOTION

ABSTRACT

This thesis presents a dynamic analysis of a biped walking robot platform, RUBI-2. RUBI-2 consists of a trunk and two legs with 12 DOF (degree of freedom) which is developed according to our design philosophy of lightweight, modular and human-like rated small size robot design for this thesis. Firstly, well-known humanoid biped robot gait generation methods are analyzed, and then an appropriate walking pattern is created. Next, a walking control strategy is defined and online controllers are developed. Walking patterns and robot balance controls are provided by using force and inertial sensor feedbacks. Finally, the performance of humanoid biped walking patterns and stability control methods are experimentally tested on humanoid biped platform RUBI-2, and dynamically balanced walking of biped robot is realized.

Keywords: Walking pattern generation, walking robot control, zero moment point, biped robot, center of pressure

İNSAN BENZERİ HAREKET İÇİN HAFİF VE MODÜLER İKİ BACAKLI ROBOT TASARIMI VE UYGULAMASI

ÖZ

Bu tez iki bacaklı yürüyen robot platformu, RUBI-2'nin dinamik analizlerini sunmaktadır. RUBI-2, bir gövde ve 12 (SD) serbestlik derecesinde iki bacaktan oluşmuş, bizim hafif, modüler ve insan ölçüleriyle orantılı olan küçük ebatlı robot tasarım felsefemize göre bu tez için geliştirilmiştir. İlk olarak, herkesçe bilinen insansı iki ayaklı robot yürüyüş biçimi üretim yöntemleri analiz edilmiş ve ondan sonrada en uygun yürüyüş eğrileri yaratılmıştır. Sonra, yürüyüş kontrol stratejisi belirlenmiş ve çevrim içi kontrolcüler geliştirilmiştir. Yürüyüş yörüngeleri ve robot denge kontrolleri, kuvvet ve eğim sensörleri aracılığı ile sağlanmıştır. Son olarak, insansı iki bacaklı robot yürüyüş yörüngelerinin ve denge kontrol metotlarının performansı, insansı iki bacaklı robot platformu RUBI-2 üzerinde deneysel olarak test edilmiş ve iki bacaklı robotun dinamik olarak dengeli yürüyüşü gerçekleştirilmiştir.

Anahtar kelimeler: Yürüyüş yörüngesi üretimi, yürüyen robot kontrolü, sıfır moment noktası, iki bacaklı robot, basınç merkezi

CONTENTS

LIST OF FIGURES

Pages

LIST OF TABLES

Pages

CHAPTER ONE
INTRODUCTION

Researchers have been interested in movable robots for a long time. The term "robot" was coined by Czech writer Karel Čapek in his science fiction play "Rossum's Universal Robots" in 1921 (Capek, 1923; Reilly, 2011). In the beginning, the word "robot" was associated with human-like machines. In due course, robot term has been replaced by "humanoid" or "biped humanoid". Nowadays, the term "robot" describes a wide range of actuated electromechanical machines. Although the term "biped" and "humanoid" are used synonymously, the term biped only refers to the robot which has two legs while humanoid expresses a human-like robot platform.

Today, the biped humanoid robot is one of the most special research topics in the robot research society. There have been many studies on biped robots since 1970 (Golliday & Hemami, 1977; Hemami, Weimer & Koozekanani, 1973). In 1973, the construction of a human-like robot was started at the Waseda University in Tokyo, Japan. WABIAN-2 is the newest biped robot of Waseda University (Yu et al., 2006). In 1986 Honda began a robot research program, ASIMO (Hirai, Hirose, Haikawa, & Takenaka, 1998). ASIMO's latest version is a more human friendly design in the well-known humanoid robots. HRP-4 of AIST (National Institute of Advanced Industrial Science and Technology, Japan) and KHR-3 of KAIST (Korea Advanced Institute of Science and Technology) are the other well-known biped humanoid robot platforms (Kaneko et al., 2011; Park, Kim, & Oh, 2006) shown in Figure 1.1.

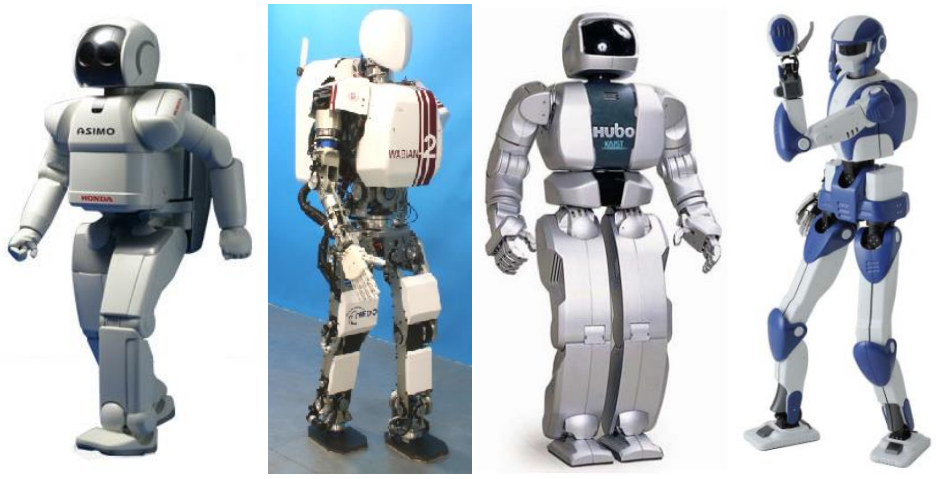

Figure 1.1 ASIMO, WABIAN-2, KHR-3: HUBO, HRP-4.

Although it is not hard to build a human-like robot, the realization of a dynamically stable, walking biped robot is a considerable challenge. At the beginning of walking robot studies, researchers involved static walking with low walking speed (Miller, 1994). For the balance strategy, the use of COG (Center of Gravity) was focused. The static walking motion was too slow, and it was depending on widely changing of COG, thus researchers began to focus on dynamic walking of biped robots (Hirai et al., 1998; Kajita et al., 2003; Qiang et al., 2001). If the dynamic balance can be maintained, robot walking becomes smoother and faster. During dynamic walking, if the inertial forces generated from the acceleration of the robot body are not controlled, a biped robot may fall down easily. In order to control inertial forces, some notions have been introduced, which are ZMP (Zero Moment Point), CoP (Center of Pressure) and FIR (Foot Indicator Point) (Goswami, 1999; Vukobratovic & Borovac, 2004).

1.1 Goal of The Thesis

At present, biped humanoid robot research groups have been supported by governments, universities and industry leaders. They all have developed their own robot platforms and walking control strategies. These sophisticated robot platforms are not easy to use for academic research due to its mechanical and electronic complexity and high production costs. Operations of the robot platforms require the attendance of qualified experts. Furthermore; because of the size and weight, the

robots are required a team of operator. Thus, for researchers, it is not easy to implement and test new algorithms by themselves.

With mentioned circumstances above, novice researchers need to have small-size, cheap and easily operated biped humanoid platforms. Therefore, the goal of this thesis is to design and develop a small-size, modular and low-cost biped robot to implement the theories of biped walking and control methods. Also, it is aimed to reach the smallest foot length to leg length ratio as possible. This ratio directly affects the dynamic stability of a robot. Both the general dimensions and the foot length to leg length ratio of the biped robot and human are shown in Table 1.1. For the development of such biped platforms, walking pattern generation methods and control system of the platforms are discussed in this work.

Table 1.1 The general dimensions and the foot length to leg length ratio of the biped robot and human.

	Height (mm)	**Leg length**	**Foot length**	**Foot width**	**Foot length to leg length ratio**	**Foot width to leg length ratio**
Human	1800	938	263	90	0.28	0.10
Asimo	1200	600	200	150	0.33	0.25
KHR-3	1200	600	233	140	0.39	0.23
RUBI-2	-	481	110	60	0.23	0.12

1.2 Thesis Organization

The remainder of this thesis is organized as follows. Chapter 2 gives a condensed summary of the tutorial on biped humanoid robot walking. Chapter 3 presents two well-known humanoid biped robot gait generation methods. Chapter 4 explains the design and mechanical realization of a biped robot RUBI-2. Chapter 5 introduces the common online control methods that are used in biped robots. Also, proposed robot control strategy is given in this chapter. Chapter 6 is devoted to the simulation of the biped robot motion. In Chapter 7, the implementation of the proposed walking pattern generations and control methods and the experiments with the biped robot RUBI-2 are given. The conclusions and recommended future work are outlined in Chapter 8.

CHAPTER TWO
BACKGROUND

The human locomotion system is the main model for the arrangement of bipedal robots. Human body is very complicated skeleton structure. Especially, the human upper body has determined human gait is the specific kinematic chain of hip, knee, ankle and foot. Human legs have many degrees of freedom (DoF) and flexibility. Therefore, creating dynamic model like a human is a challenging study.

As shown in Figure 2.1, human motion is examined on three planes. If the motion of human are analyzed plane by plane, understanding the human gait become easier. Gait analysis is done on two or more planes within the sagittal, frontal and transverse plane to achieve dynamic motions of biped robot. The largest numbers of important articulations exist on the sagittal plane. Like a human, most of the movement in robot walking mainly takes place in this plane.

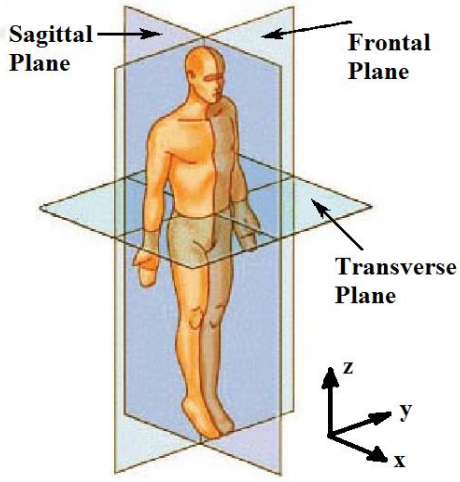

Figure 2.1 Human body planes.

The locomotion system of biped robot generally is 12 degree of freedom (DoF) that is required minimum for human-like locomotion. For each leg, there are 3 DoF in the hip joint, 1 DoF in the knee joint, and 2 DoF in the ankle joint.

This chapter gives a condensed summary of the tutorial in biped humanoid robot walking.

2.1 Biped Gait

Biped walking is a periodic phenomenon. A one cycle of humanoid robot walking is divided into two main phase: a single support phase (SSP) and a double support phase (DSP). In the single support phase, the one foot is swinging forward through the air while other foot is in contact with the ground. On the other hand both humanoid robot feet are stationary on the ground in the double-support phase. The SSP starts with the toe of the rear foot leaving the ground, and finishes when the heel of the forward foot touching the ground. The DSP starts with the heel of the forward foot touching the ground, and finishes when the toe of the rear foot leaving the ground. Phase of biped gait on sagittal and frontal planes are shown in Figure 2.2.

If the DSP time is too short, the CoM of robot has to move too fast. In other words, ZMP must be transferred from the one foot to the other foot too fast. This situation affects robot's stability negatively. On the other hand, if the DSP time is too long, the robot cannot walk at high speed (Qiang et al., 2001). The interval of double-support phase in human motion is about %20 (Inman, Ralston, Todd, & Lieberman, 1981; McMahon, 1984).

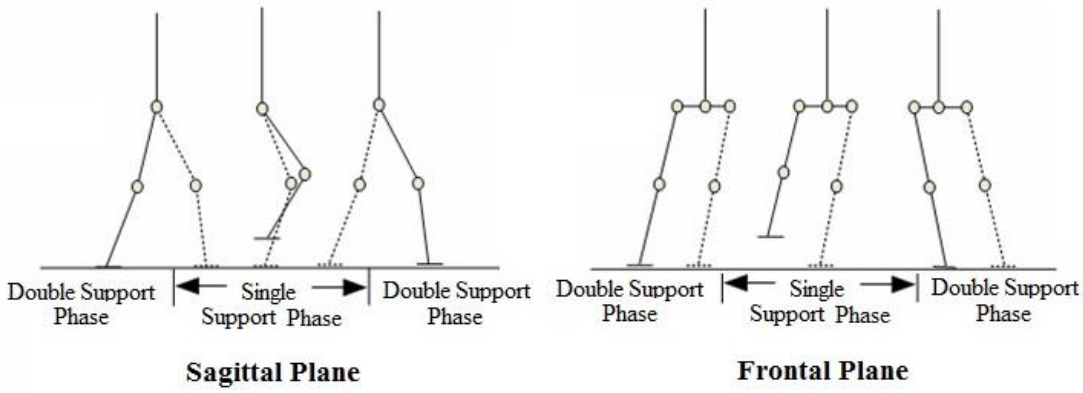

Figure 2.2 Phase of biped gait on sagittal and frontal planes.

The supporting area is introduced by the convex hull about the ground support points. Figure 2.3 shows the supporting area in single and double support phase. During the single support phase, the supporting area is one foot ground contact area. In the double support phase, the supporting area is the ground contact area of both feet and the domain between them.

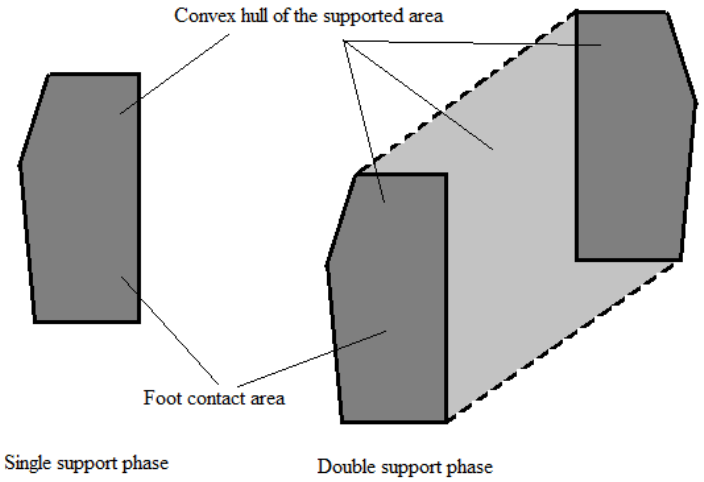

Figure 2.3 The supporting area during single and double support phase.

In the walking robots, the support foot remains at the fixed position on the ground by means of the gravitational force and friction forces. The weight of robot limits the applicable force and toque. Therefore, the supporting area is an important property for balanced biped walking.

2.2 The Ground Projection of Center of Mass (GCoM)

Only gravitational forces are acted a motionless robot. These forces can be shown as virtual force acting at the center of mass (CoM) which can be calculated by following equation:

$$p_{CoM} = \frac{\sum_i m_i p_i}{\sum_i m_i} \tag{2.1}$$

where m_i is the mass of the i'th link of the robot and p_i is the position of the i'th link mass center.

The location of CoM is a deterministic property for the balance of the robot. CoM's orthogonal projection to the ground is called the Center of gravity (CoG) or the Ground Projection of Center Of Mass (GCoM) (Kun & Miller, 1999), shown in Figure 2.4.

CoG or GCoM determines only robots static balance. If there is a dynamic motion, dynamic forces and moments become larger than static forces. Therefore, robot falls over although the CoG is exited with in the supporting area.

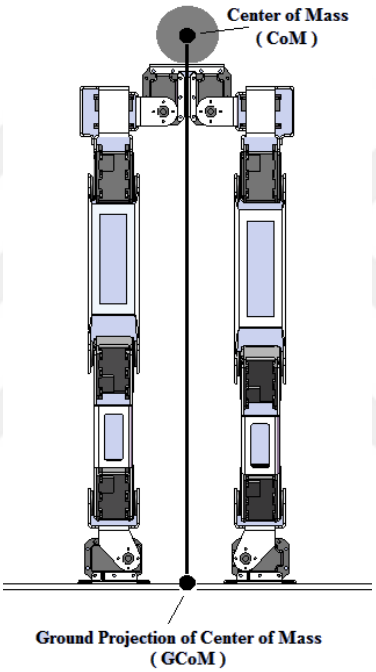

Figure 2.4 The ground projection of center of mass (GCoM).

2.3 The Center of Pressure (COP)

The foot-ground contact forces of the biped can be represented by a resultant Ground Reaction Force (GRF) that is acting at the Center of Pressure (CoP). CoP is a virtual point and does not need to the contact between the foot and the ground. In the single support phase, overall CoP is located at the one foot supporting area. While robot is moving in the double support phase, overall CoP is located between two feet. In the meantime each foot has a local CoP in their supporting areas.

CoP can be calculated by following equation:

$$p_{CoP} = \frac{\sum_i F_i p_i}{\sum_i F_i} \tag{2.2}$$

where F_i is the local foot contact force i and p_i is the point of force action. The resultant Ground Reaction Force acting at the Center of Pressure is shown in Figure 2.5.

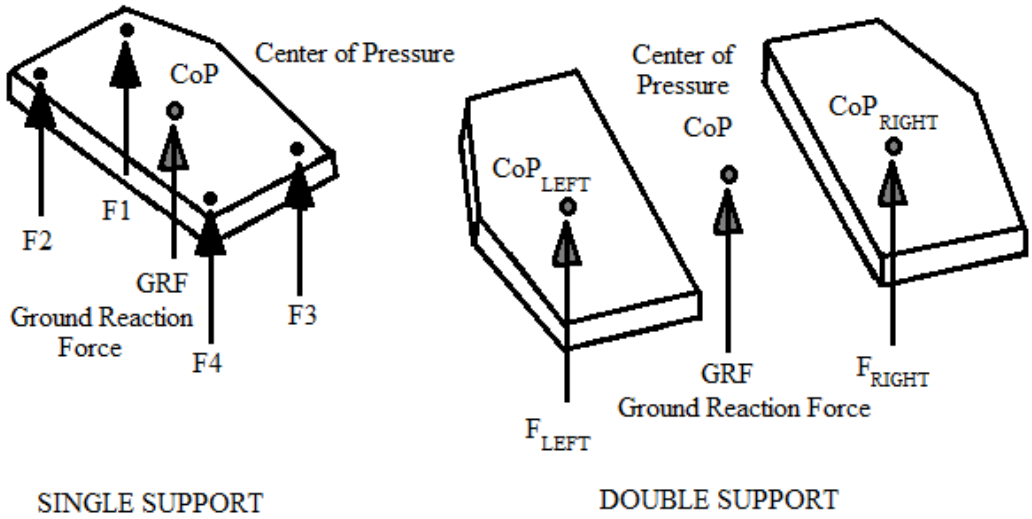

Figure 2.5 The resultant Ground Reaction Force acting at the Center of Pressure.

2.4 The Zero Moment Point (ZMP)

The zero moment point is defined as that point on the ground at which the all the moments of the inertial and gravity forces equal zero (Vukobratovic & Borovac, 2004). The ZMP is commonly used as dynamic stability criterion for humanoid biped robot walking controllers. If the ZMP is the supporting area, biped robot is dynamically stable. The coordinate of the ZPM $(x_{zpm}, y_{zpm}, 0)$ can be calculated by the following equations:

$$x_{zmp} = \frac{\sum_{i=1}^{n} m_i(\ddot{z}_i + g)x_i - \sum_{i=1}^{n} m_i \ddot{x}_i z_i - \sum_{i=1}^{n} I_{iy}\ddot{\Omega}_{iy}}{\sum_{i=1}^{n} m_i(\ddot{z}_i + g)} \tag{2.3}$$

$$y_{zmp} = \frac{\sum_{i=1}^{n} m_i(\ddot{z}_i + g)y_i - \sum_{i=1}^{n} m_i \ddot{y}_i z_i - \sum_{i=1}^{n} I_{ix}\ddot{\Omega}_{ix}}{\sum_{i=1}^{n} m_i(\ddot{z}_i + g)} \tag{2.4}$$

where m_i is the mass of link i, (x_i, y_i, z_i) is the coordinate of the center of mass, $\ddot{\Omega}_{ix}$ and $\ddot{\Omega}_{iy}$ are the absolute angular velocity component around x–axis and y -axis at the center of gravity, $(\ddot{x}_i, \ddot{y}_i, \ddot{z}_i)$ is the accelerations of the center of mass, I_{ix} and I_{iy} are the inertial components for each of link i and g is the gravity on the Cartesian coordinate system.

The minimum distance (d_{zpm}) between the ZMP and the boundary of the stable region (supported foot area) is called the stability margin, shown in Figure 2.6.

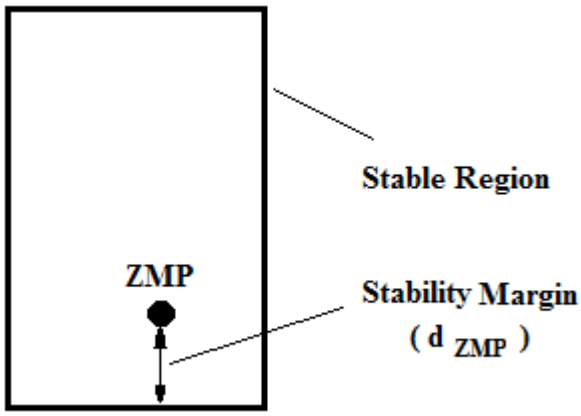

Figure 2.6 The stability margin for ZMP.

In researches, Goswami (1999), introduced the notion of foot rotation indicator (FRI). Goswawi's FRI and CoP approaches are similar to ZMP and imaginary ZMP (Vukobratovic & Borovac, 2004) (Figure 2.7). The ZMP is easy to compute hence is used for gait generation. The CoP is easy to measure therefore is used for control of robot.

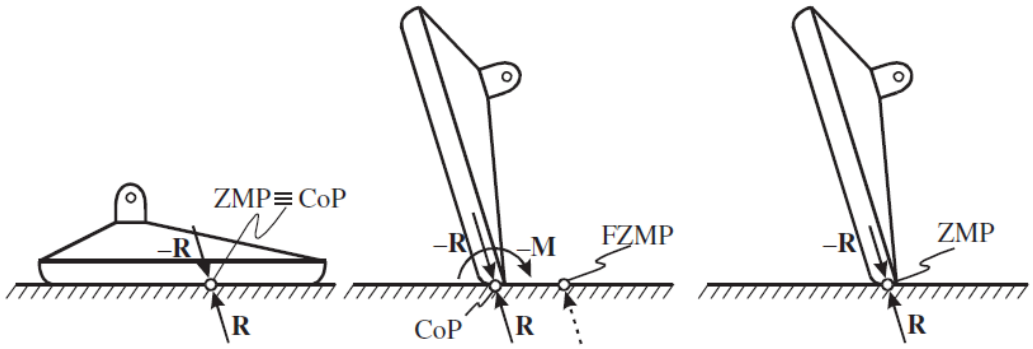

Figure 2.7 Relations between ZMP and CoP (Vukobratovic & Borovac, 2004).

2.5 Static and Dynamic Balance

A biped walking robot can tip over easily by reason of body structure and high DoF. For this reason, stability is a primary requirement for the biped robot walking trajectory generation. There are two type stability of biped robot locomotion. The first type is called static stability and it applies when biped robot moves slowly. The second type is called dynamic walking stability and it applies when biped robot moves faster speed.

During the robot motion, forces like inertial, gravitational, centrifugal and Coriolis effect the robot balance. Especially, dynamic forces dominate static forces with increasing biped walking speed. These dynamic forces can be neglected in slow walking speed. If the ZMP and GCoM always remain within the supporting area, the motion of robot is called statically balanced. If the ZMP remain within the supporting area while GCoM leaves from the supporting area, the motion of robot is called dynamically balanced (Ching-Long, 1999; Zhe, Changjiu, & Zenqi, 2003).

2.6 Robot Control Strategies

There are two different approaches to biped walking control strategies. First strategy assumes that accurate model of robot can be created with environments. Description of such a system would lead to great dynamic complexity. Second strategy is a using simplified model of robot with feedback control.

One of the most popular methods based on a simplified model is the inverted pendulum method. Numerous approaches have been studied to humanoid biped robot with the inverted pendulum approximation ref (Erbatur & Kurt, 2009; Kajita et al., 2003; Youngjin, Bum-Jae, & Sang-Rok, 2004). In this approach, it is assumed that the mass is concentrated at the CoM of the robot and the base of the pendulum coincides with the support foot as seen in Figure 2.8. An approximate position of foot can be calculated in order to body motion.

Difference between calculated motion and real motion of robot must be compensated by feedback control. More detailed descriptions of the inverted pendulum approach and feedback control methods are given in Section 3 and Section 5 respectively.

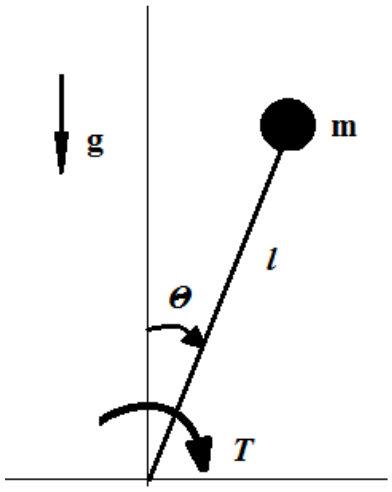

Figure 2.8 The inverted pendulum model.

Qiang et al. (2001), proposed different approach to generate robot motion. In this method, the constraints of the foot motion parameters were formulated with smooth hip motion. The foot motion was specified with some constrain like foot landing position, maximum height of swing foot, ground conditions. After that the foot trajectories were generated using cubic spline interpolation method. More detailed descriptions of this method are given in Section 3.

CHAPTER THREE
WALKING PATTERN GENERATION

This chapter presents two well-known humanoid biped robot gait generation methods. In order to achieving biped walking, suitable walking trajectories are calculated and replay on the robot. Generation of walking patterns can be calculated online as well as offline. At offline method, the robot selects one of precalculated trajectories according to the situation.

These methods generally present to obtain the foot and hip trajectories to achieve the walking of the robot. In order to reach the robot links dynamics, it is needed to apply inverse kinematics.

3.1 Walking Pattern Generation by The Foot Parameters

In this method, the constraints of the foot motion parameters were formulated to adapt to ground conditions. Then, the formulations are integrating with generation of smooth hip motion. The largest numbers of important articulations of biped robot are occurred in the sagittal plane. Hence, method is focused on sagittal plane.

Determination of foot trajectories and hip trajectories are enough to explain the walking pattern of biped robot. Then, joint angles of the biped robot are calculated by using invers kinematics.

Qiang et al. (2001), expressed foot trajectories by a vector X_a = [$x_a(t)$, $z_a(t)$, $\theta_a(t)$]^T, where ($x_a(t)$, $z_a(t)$) is the coordinate of the ankle position, and $\theta_a(t)$ is the angle of the foot. Also hip trajectory was expressed by a vector X_h = [$x_h(t)$, $z_h(t)$, $\theta_h(t)$]^T, where ($x_h(t)$, $z_h(t)$) is the coordinate of the hip position, and $\theta_h(t)$ is the angle of the hip, shown in Figure 3.1.

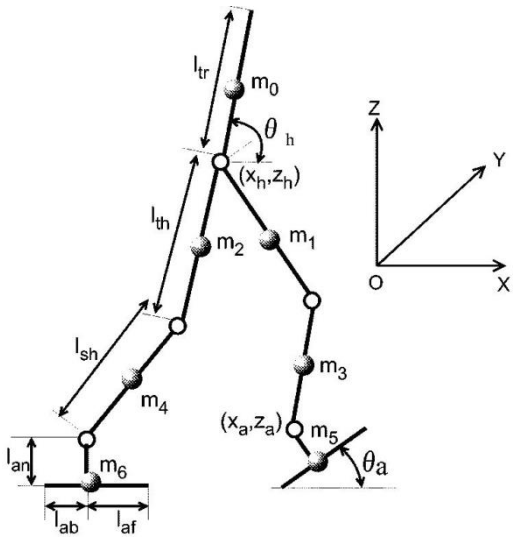

Figure 3.1 Model of the biped robot (Qiang et al., 2001).

3.1.1 Foot Trajectories

Only one foot trajectory calculations were expressed in this method. For complete walking cycle, the calculated foot trajectories are used as other foot trajectory with a delay.

The walking step starts when the heel of the swing foot leaving the ground and finishes when the heel of the swing foot touching the ground. The period of one walking step is T_c and k = 1, 2, 3…,K, K is the number of step.

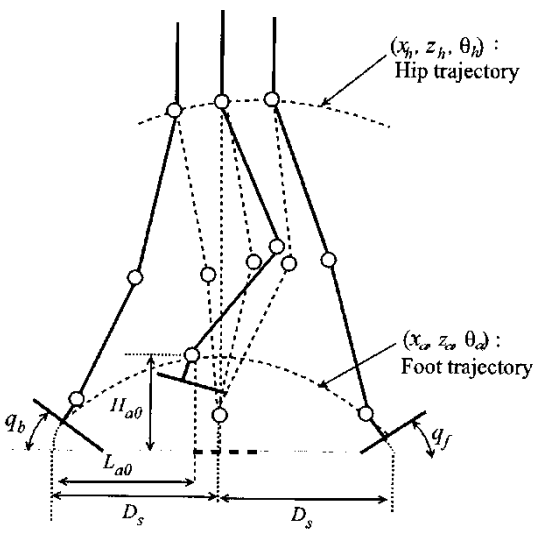

Figure 3.2 Walking parameters of biped robot (Qiang et al., 2001).

T_d is the interval of the double-support phase. q_b and q_f are the angles of foot when it leaves and lands on the ground as shown in Figure 3.2. It is assumed that the sole of the swing foot is in contact with the ground and following constrains are obtained for $\theta_a(t)$:

$$\theta_a(t) = \begin{cases} q_{gs}(k), & t = kT_c \\ q_b, & t = kT_c + T_d \\ -q_f, & t = (k+1)T_c \\ -q_{ge}(k), & t = (k+1)T_c + T_d \end{cases} \tag{3.1}$$

where $q_{gs}(k)$ and $q_{ge}(k)$ are the angles of the ground surface which under the support foot. $q_{gs}(k) = q_{ge}(k) = 0$, if the support foot is on level ground.

If there are obstacles in environments, the swing foot position is important to pass away them. Letting L_{ao} and H_{ao} are the positions of the highest point of the swing foot and T_m is the time that the swing foot reaches the highest position, above constrains are obtained for $x_a(t)$:

$$x_a(t) = \begin{cases} kD_s, & t = kT_c \\ kD_s + l_{an}\sin q_b + l_{af}(1-\cos q_b), & t = kT_c + T_d \\ kD_s + L_{ao}, & t = kT_c + T_m \\ (k+2)D_s - l_{an}\sin q_f - l_{ab}(1-\cos q_f), & t = (k+1)T_c \\ (k+2)D_s, & t = (k+1)T_c + T_d \end{cases} \tag{3.2}$$

and for $z_a(t)$:

$$z_a(t) = \begin{cases} h_{gs}(k) + l_{an}, & t = kT_c \\ h_{gs}(k) + l_{af}\sin q_b + l_{an}\cos q_b, & t = kT_c + T_d \\ H_{ao}, & t = kT_c + T_m \\ h_{ge}(k) + l_{ab}\sin q_f + l_{an}\cos q_f, & t = (k+1)T_c \\ h_{ge}(k) + l_{an}, & t = (k+1)T_c + T_d \end{cases} \tag{3.3}$$

where D_s is the length of one step (Figure 3.2), $h_{gs}(k)$ and $h_{ge}(k)$ are the heights of the ground surface which under the support foot, l_{an} is the height of the foot, l_{af} is the length from the ankle joint to the toe and l_{ab} is the length from the ankle joint to the heel (Figure 3.1). $h_{gs}(k)$ = $h_{ge}(k)$ = 0, if the support foot is on level ground.

To obtain a smooth trajectory, it is necessary that the first derivatives (velocity) terms $\dot{x}_a(t)$, $\dot{z}_a(t)$ and $\dot{\theta}_a(t)$ be differential. Also acceleration (second derivatives) terms $\ddot{x}_a(t)$, $\ddot{z}_a(t)$ and $\ddot{\theta}_a(t)$ be continuous at all breakpoints t. In addition, the first derivatives terms $\dot{x}_a(t)$, $\dot{z}_a(t)$ and $\dot{\theta}_a(t)$ be zero at $t = kT_c$ and $t = (k+1)T_c + T_d$.

Due to computation difficulties and high degrees, using polynomial interpolation is not practical. However, if there is a usage of third-order interpolation, the second derivatives $\ddot{x}_a(t)$, $\ddot{z}_a(t)$ and $\ddot{\theta}_a(t)$ are always continuous. Therefore, to satisfy above conditions, using third-order interpolation is best way to find $x_h(t)$, $z_h(t)$ and $\theta_h(t)$ (Qiang et al., 2001).

3.1.2 Hip Trajectories

The important parameter is stability and the ZMP when determining the hip motion. The angle of the hip $\theta_h(t)$ is selected constant when there is no upper body. The change of motion $z_h(t)$ hardly affects the position of the ZPM. Therefore,

$z_h(t)$ can be chosen constant or within a fixed range. If $z_h(t)$ is chosen within a fixed range, above constrains are obtained:

$$z_h(t) = \begin{cases} H_{h\min}, & t = kT_c + 0.5T_d \\ H_{h\max}, & t = kT_c + 0.5(T_c - T_d) \\ H_{h\min}, & t = (k+1)T_c + 0.5T_d \end{cases} \tag{3.4}$$

where $H_{h\max}$ is the highest position of the hip at the middle of the SSP and $H_{h\min}$ is the lowest position of the hip at the middle of the DSP.

The change of $x_h(t)$ directly affects the stability of a biped robot. To obtain desired ZMP trajectories, the following method is proposed by Qiang et al. (2001). x_{sd} and x_{ed} are important parameter to reach $x_h(t)$ trajectory. Thus, above constrains are obtained for $x_h(t)$:

$$x_h(t) = \begin{cases} kD_s + x_{ed}, & t = kT_c \\ (k+1)D_s - x_{sd}, & t = kT_c + T_d \\ (k+1)D_s + x_{ed}, & t = (k+1)T_c \end{cases} \tag{3.5}$$

To satisfy a smooth trajectory, third-order interpolation is used. Where, x_{sd} is distance from the hip to the ankle of the support foot at the start of the SSP. x_{ed} is distance from the hip to the ankle of the support foot at the end of the SSP on the sagittal plane, as shown in Figure 3.3. x_{sd} and x_{ed} are described for a range in equations (3.6).

$$\begin{cases} 0,0 < x_{sd} < 0,5D_s \\ 0,0 < x_{ed} < 0,5D_s \end{cases} \tag{3.6}$$

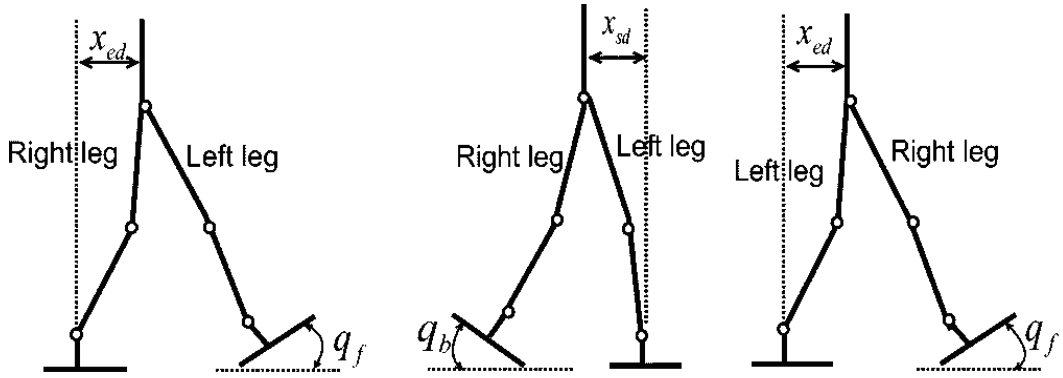

Figure 3.3 Hip position of the biped robot in the walking cycle (Qiang et al., 2001).

3.2 Linear Inverted Pendulum Model

The Linear Inverted Pendulum Model (LIPM) introduces a simplified model for a biped robot, as shown in Figure 3.4. This simplified model is assumed that the motion of CoM moves in fixed height surface. Also it is assumes that all mass concentrated in one point at the biped CoM. Where, the mass of legs is negligible respect to the biped robot trunk.

Youngjin et al. (2004), are proposed to use The Linear Inverted Pendulum Model (LIPM) with fixed Zero Moment Point (ZMP) to generate walking pattern. This method is examined a finding center of mass (CoM) position with the given ZMP reference.

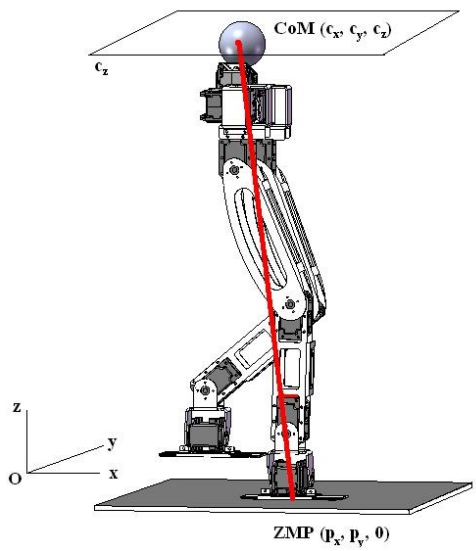

Figure 3.4 LIPM model of biped robot.

In Figure 3.4, the position CoM is described by (c_x,c_y,c_z) and the ZMP is described by point on supporting foot (p_x,p_y,0). Where, c_z is the fixed moving height of CoM, m is the mass of biped robot and g is the gravity constant. The equations of motion are obtained as:

$$\tau_x = mgc_y - m\ddot{c}_y c_z \tag{3.7}$$
$$\tau_y = -mgc_x + m\ddot{c}_x c_z \tag{3.8}$$
$$\tau_z = -m\ddot{c}_x c_y + m\ddot{c}_y c_x \tag{3.9}$$

where τ_i is the moment about i-coordinate axis for i=x,y,z. The definition of ZMP is introduced as following forms:

$$p_x = -\frac{\tau_y}{\mathrm{mg}} \tag{3.10}$$
$$p_y = -\frac{\tau_x}{\mathrm{mg}} \tag{3.11}$$

The equations of ZMP can be obtained from equations 3.7 and 3.8 as follows:

$$\mathrm{p_x} = \mathrm{c_x} - \frac{\mathrm{c_z}}{\mathrm{g}}\ddot{\mathrm{c}}_\mathrm{x} \tag{3.12}$$
$$\mathrm{p_y} = \mathrm{c_y} - \frac{\mathrm{c_z}}{\mathrm{g}}\ddot{\mathrm{c}}_\mathrm{y} \tag{3.13}$$

It is mentioned that while the swing foot is moving, ZMP should be on the supporting foot area for robot stability. In double support phase, ZMP should be moved from one foot to the other. This action should be repeated for stable walking. Therefore, Youngjin et al. (2004), worked on the reference ZMP trajectory can be used for generating walking pattern. It is assumed that ZMP is always on the middle of supporting foot in the SSP and moves quickly to the other foot in the DSP. The reference ZMP trajectories are shown in Figure 3.5 and 3.6.

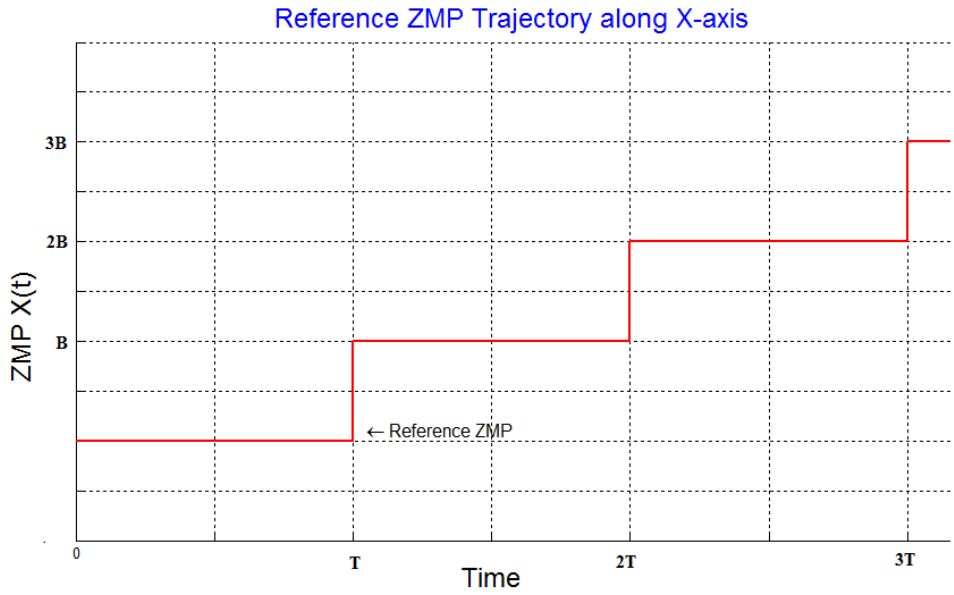

Figure 3.5 Reference ZMP p_x,

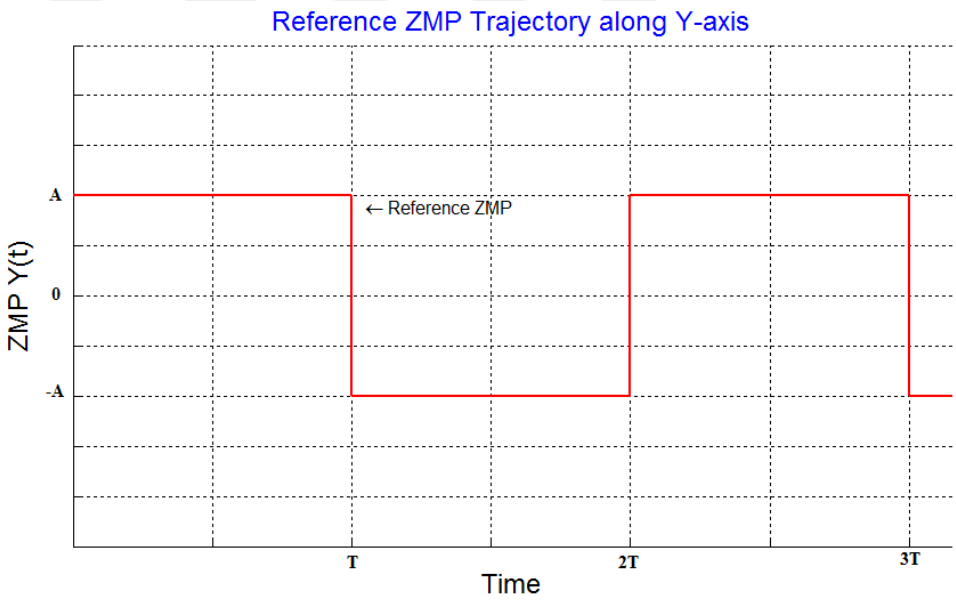

Figure 3.6 Reference ZMP p_y.

The following transfer function can get from equations (3.12) and (3.13):

$$C_i(s) = \frac{1}{1-(c_z/g)s^2}\left[P_i(s) - \left(\frac{c_z}{g}\right)c_i(0)s - \left(\frac{c_z}{g}\right)\dot{c}_i(0)\right] \tag{3.14}$$

for i = x,y, where $C_i(s)$ and $P_i(s)$ are the Laplace transformations of $c_i(t)$ and $p_i(t)$, $c_i(0)$ and $\dot{c}_i(0)$ are the initial conditions of trajectory of CoM. The reference ZMP assumed in Figure 3.5 and 3.6 can be expressed as:

$$p_x^{ref}(t) = \mathrm{B}\sum_{k=1}^{\infty} u(t - kT_0) \tag{3.15}$$
$$p_y^{ref}(t) = A1(t) + 2\mathrm{A}\sum_{k=1}^{\infty}(-1)^k u(t - kT_0) \tag{3.16}$$

where $u(t - kT_0)$ is the unit-step functions starting at t = kT_o. A expresses the distance between two feet centers in y direction. B expresses the step distance in x direction. If the equations of (3.15) and (3.16) are applied to the equation (3.14) with zero initial conditions:

$$C_x(s) = \frac{1}{1-(c_z/g)s^2}\left[\frac{B}{s}e^{-T_0 s} + \frac{B}{s}e^{-2T_0 s} + \frac{B}{s}e^{-3T_0 s} + \cdots\right] \tag{3.17}$$
$$C_y(s) = \frac{1}{1-(c_z/g)s^2}\left[\frac{A}{s} - \frac{2A}{s}e^{-T_0 s} + \frac{2A}{s}e^{-2T_0 s} - \frac{2A}{s}e^{-3T_0 s} + \cdots\right] \tag{3.18}$$

by letting $w_n^2 = g/c_z$, it is known that:

$$\frac{1}{1-\left(\frac{c_z}{g}\right)s^2}\cdot\frac{1}{s} = \frac{1}{s} - \frac{s}{s^2 - w_n^2} \tag{3.19}$$

the transfer functions are rearranged as a follows:

$$C_x(s) = B\left(\frac{1}{s} - \frac{s}{s^2-w_n^2}\right)e^{-T_0 s} + B\left(\frac{1}{s} - \frac{s}{s^2-w_n^2}\right)e^{-2T_0 s} + B\left(\frac{1}{s} - \frac{s}{s^2-w_n^2}\right)e^{-3T_0 s} + \cdots \tag{3.20}$$
$$C_y(s) = A\left(\frac{1}{s} - \frac{s}{s^2-w_n^2}\right) - 2A\left(\frac{1}{s} - \frac{s}{s^2-w_n^2}\right)e^{-T_0 s} + 2A\left(\frac{1}{s} - \frac{s}{s^2-w_n^2}\right)e^{-2T_0 s} - 2A\left(\frac{1}{s} - \frac{s}{s^2-w_n^2}\right)e^{-3T_0 s} + \cdots \tag{3.21}$$

Finally the exact reference trajectories of the CoM are obtained by using the inverse Laplace transformations as:

$$c_x(t) = B[1 - \cosh w_n(t - T_0)]u(t - T_0) + B[1 - \cosh w_n(t - 2T_0)]u(t - 2T_0) + B[1 - \cosh w_n(t - 3T_0)]u(t - 3T_0) + \cdots$$
$$c_x(t) = \mathrm{B}\sum_{k=1}^{\infty}[1 - \cosh w_n(t - kT_0)]u(t - kT_0) \tag{3.22}$$

$$c_y(t) = A[1-\cosh w_n(t)] - 2A[1-\cosh w_n(t-T_0)]u(t-T_0) + 2A[1-\cosh w_n(t-2T_0)]u(t-2T_0) - 2A[1-\cosh w_n(t-3T_0)]u(t-3T_0) + \cdots$$

$$c_y(t) = A[1-\cosh w_n(t)] + 2\mathrm{A}\sum_{k=1}^{\infty}(-1)^k[1-\cosh w_n(t-kT_0)]u(t-kT_0) \quad (3.23)$$

Although these reference trajectories of the CoM are exact solutions for the differential equations (3.12) and (3.13), they are difficult to use for biped walking robots because of the unbounded functions cosh. In addition, they are numerically unstable and very sensitive to variation of W_n. Therefore, Youngjin et al. (2004) suggest a CoM trajectory planning method by using Fourier series. This method is the approximate solution of $c_x(t)$ and $c_y(t)$.

3.2.1 Approximate Solution of $c_x(t)$ and $c_y(t)$

In this approximate solution method with Fourier series, reference ZMP p_x^{ref} and p_y^{ref} are introduced the odd functions with period T_o. Also, reference CoM trajectories c_x^{ref} and c_y^{ref} are expressed as Fourier series.

x- directional reference CoM trajectory is expressed as Fourier series form.

$$c_x^{ref}(t) = \frac{\mathrm{B}}{T_0}\left(t-\frac{T_0}{2}\right) + \sum_{n=1}^{\infty}\left(a_n\cos\frac{n\pi t}{T_0} + b_n\sin\frac{n\pi t}{T_0}\right) \quad (3.24)$$

The coefficients a_n =0 and b_n can be obtained by solving odd function p_x^{ref}.

$$b_n = \frac{\mathrm{B}T_0^2 w_n^2(1+\cos n\pi)}{n\pi(T_0^2 w_n^2 + n^2\pi^2)} \quad (3.25)$$

Finally, x- directional reference CoM trajectories c_x^{ref} can be obtained as follows:

$$c_x^{ref}(t) = \frac{\mathrm{B}}{T_0}\left(t-\frac{T_0}{2}\right) + \sum_{n=1}^{\infty}\frac{\mathrm{B}T_0^2 w_n^2(1+\cos n\pi)}{n\pi(T_0^2 w_n^2 + n^2\pi^2)}\sin\frac{n\pi t}{T_0} \quad (3.26)$$

Also, y- directional reference CoM trajectory is expressed as Fourier series form.

$$c_y^{ref}(t) = \frac{a_0}{2} + \sum_{n=1}^{\infty} \left(a_n \cos\frac{n\pi t}{T_0} + b_n \sin\frac{n\pi t}{T_0} \right) \tag{3.27}$$

The coefficients a_n =0 and b_n can be obtained by solving odd function p_y^{ref}.

$$b_n = \frac{2AT_0^2 w_n^2 (1-\cos n\pi)}{n\pi(T_0^2 w_n^2 + n^2\pi^2)} \tag{3.28}$$

Finally, y- directional reference CoM trajectories c_y^{ref} can be obtained as follows:

$$c_y^{ref}(t) = \sum_{n=1}^{\infty} \frac{2AT_0^2 w_n^2 (1-\cos n\pi)}{n\pi(T_0^2 w_n^2 + n^2\pi^2)} \sin\frac{n\pi t}{T_0} \tag{3.29}$$

Figure 3.7 and 3.8 show the reference CoM trajectories with the reference ZMP and Fourier approximation reference ZMP.

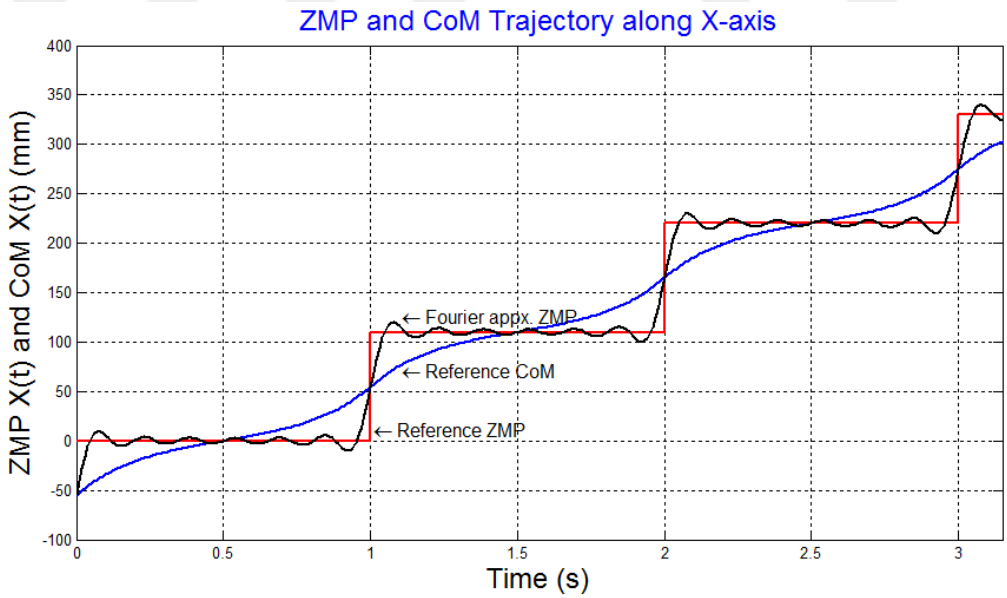

Figure 3.7 The reference CoM trajectories c_x^{ref} with Reference ZMP p_x and Fourier approximation reference ZMP p_x^{ref} for n = 12.

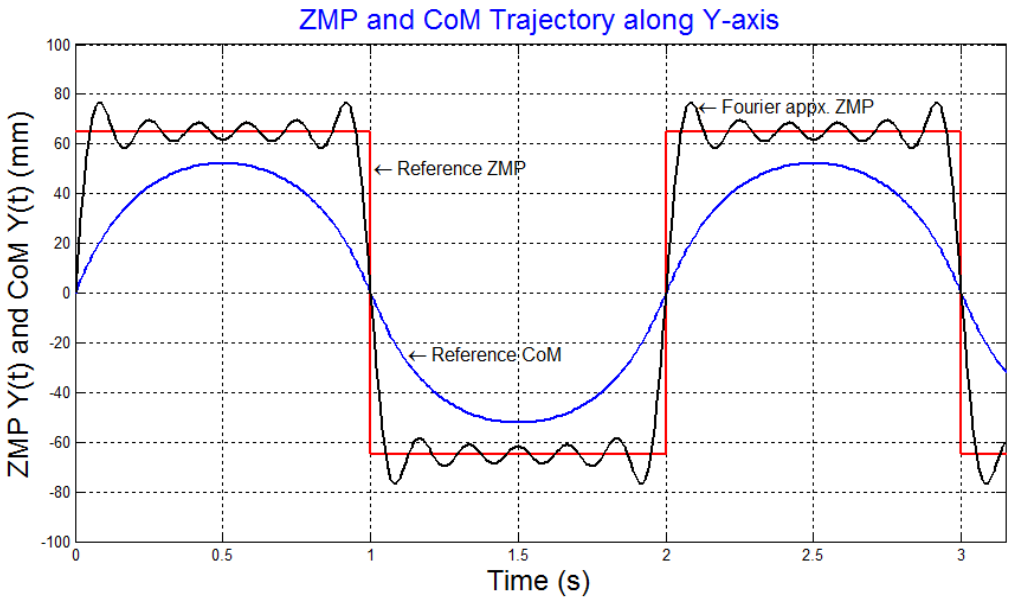

Figure 3.8 The reference CoM trajectories c_y^{ref} with Reference ZMP p_y and Fourier approximation reference ZMP p_y^{ref} for n = 12.

Although Fourier series have Gibbs phenomenon (Erbatur & Kurt, 2009) and the reference ZMP have a small double support phase, approximate solution of CoM references are suitable for using biped robot applications.

CHAPTER FOUR
BIPED ROBOT PLATFORM

In this chapter, the design and mechanical realization of a biped robot RUBI-2 are presented. It is mentioned that the goal of this thesis is the design and developing of a small-size, modular and low-cost biped robot. Although, human-like moving humanoid robots are possible to produce technically, real human walking model cannot be applied practically today. Since, the human walking has a complex dynamic movement due to high degree of freedom and deformable complex body structure.

The robot performance achieved is hardly depending on the design of the biped robot. Weight of robot, motor-gear combinations, and lower body DoF are directly affect the success of biped robot. Also, sensors used, their localizations and software environment are also important to the control system of robot.

The organization of this chapter is as follows: Section 4.1 describes the kinematic structure of the biped robot with actuators. Electronic hardware, used sensors and the software environment are described in Section 4.2.

4.1 Design of Biped Robot RUBI-2

Biped robot RUBI-2 is designed according to human lower body shape with a trunk. RUBI-2 was developed with the design philosophy that is a kinematically simple structure, human like movements, low power consumption, compact size and lightweight. CAD model of biped robot and realized biped robot RUBI-2 are shown in Figure 4.1.

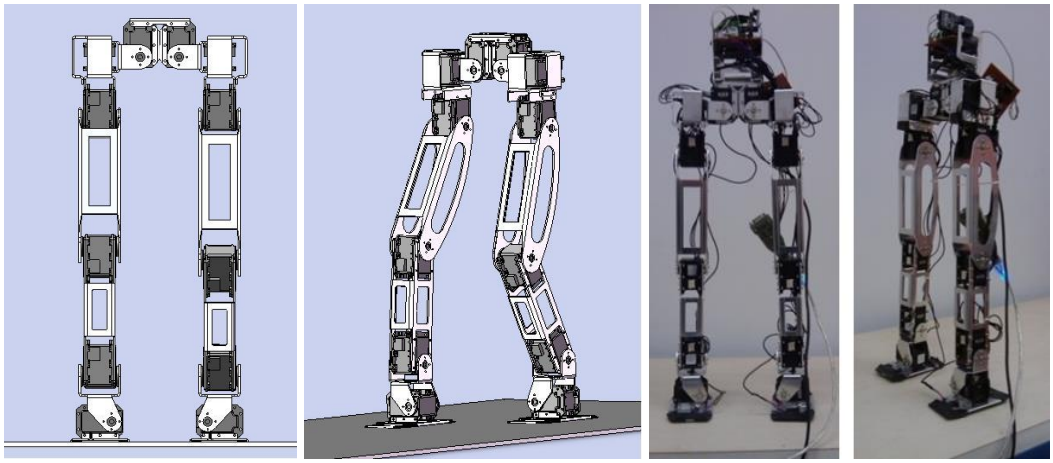

Figure 4.1 CAD model of biped robot and realized biped robot RUBI-2.

The locomotion system is selected to 12 degrees of freedom (DoF) as shown in Figure 4.2. The degrees of freedom of the biped robots are shown in Table 1.

Table 4.1 Degrees of freedom of biped robot RUBI-2.

Joint	**Direction**	**Degrees of freedom**
Hip	x, y, z	3 d.o.f. × 2 = 6 d.o.f.
Knee	y	1 d.o.f. × 2 = 2 d.o.f.
Ankle	x.y	2 d.o.f. × 2 = 4 d.o.f.
		12 d.o.f.

Figure 4.2 The joint structure of biped robot RUBI-2.

Biped robot RUBI-2 is modeled with 1/2.3 the proportion of human lower body. The general dimensions of the biped robot are shown in Table 4.2.

Table 4.2 General dimensions of RUBI-2.

Height	481 mm
Width	190 mm
Depth	68 mm
Length of a thigh (the hip to the knee)	232 mm
Length of a shin (the knee to the ankle)	141 mm
Length of a ankle (the ankle to the foot)	72 mm

RUBI-2 power requirement is supplied by 14.8 V 4200 mA Li-Po battery at the trunk. Li-Po battery is placed on the hip motors in order to ensure CoM height minimum as shown Figure 4.6.

Table 4.3 shows the other physical parameters of RUBI-2.

Table 4.3The other physical parameters of RUBI-2.

Length (cm)	l_{tr}	l_{th}	l_{sh}	l_{an}	l_{ab}	l_{af}	
	11	15.8	14.1	7.1	5	6	
Mass (gram)	m_0	m_1	m_2	m_3	m_4	m_5	m_6
	215	110	110	185	185	95	95

4.1.1 Joint Actuators

As joint actuators, Dynamixel RX-28 smart robot servos (Figure 4.3) are used. Dynamixel robot actuators are high-performance geared actuators with various sensors embedded, controlled by digital packet communication. These actuators are connected each other with daisy chain by their integrated controller. It becomes easy to control of motor at the complex assemblies. Table 4.4 is shows the specifications of Dynamixel RX-28 servos.

Figure 4.3 Dynamixel RX-28 servos.

Table 4.4 The specifications of Dynamixel RX-28 servos.

Dimensions	Length x Breadth x Height 50.6 mm x 35.6 mm x 35.5 mm
Torque	28.3 kg.cm @ 12 V (37.7 kg.cm @ 16V)
Speed	0.167 sec./60 degrees @ 12 V(0.126 sec./60 degrees @ 16 V)
Operating Angle	300 degrees for servo mode, 360 degrees for wheel mode
Operating Voltage	11-16 V
Gear Ration	1:193
Weight	72 grams

4.2 Electronic Hardware

4.2.1 USB2Dynamixel

USB2Dynamixel is a device used to operate Dynamixel actuators directly from PC (Figure 4.4). The communication mode is RS485 communication for RX-28 actuators.

Figure 4.4 USB2Dynamixel.

4.2.2 x-IMU

The x-IMU is the inertial measurement unit platform with Bluetooth communication and auxiliary ports, shown in Figure 4.5. It is used for measuring the biped robot CoM oscillations at the RUBI-2. The x-IMU has gyroscope, accelerometer and magnetometer works in triple axis. Also, it is not affected from motors magnetic field. Table 4.5 is shows the specifications of the x-IMU.

Table 4.5 The specifications of the x-IMU.

Dimensions	Length x Breadth x Height 57 mm x 38 mm x 21 mm
Connectivity	USB, Bluetooth, Micro SD Card, UART (with auxiliary port)
Operating Voltage	3.6-6.3 V
Auxiliary Port	8 channels digital I/O mode and analog input mode
Weight	12 grams

Figure 4.5 The x-IMU.

Li-Po battery, x-IMU and Usb2dynamixel are installed to the biped robot trunk is shown in Figure 4.6.

Figure 4.6 The biped robot trunk with battery, x-imu and Usb2dynamixel.

4.2.3 Force Sensing Resistors

A force measurement system is consisted of Force Sensing Resistors (FSRs). FSRs show a decrease in voltage at the terminals when an increasing force applied to their surface. Four 0.6´´ circular FSR sensors are placed under the robot foot. Sensors are placed the four corners, as shown in Figure 4.7. Therefore, the forces acting under the foot and CoP point is obtained by force measurement units.

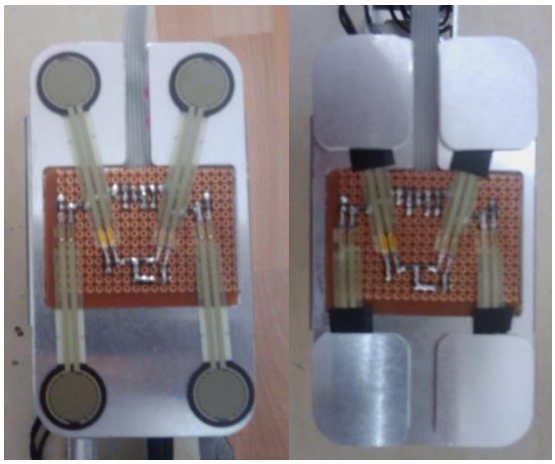

Figure 4.7 The placement of four FSR sensors.

4.2.4 The Software Environment

RUBI-2's software environment runs on a PC. Measured signals come from FSRs and IMU are transmitted the PC via the Bluetooth by x-IMU. Reference and calculated data signal come from robot controller are transmitted the biped robot via the USB bus by USB2Dynamixel. All data are processed by biped robot controller realized with MATLAB. User interface of biped robot controller is created by MATLAB Gui as shown in Figure 4.8. RUBI-2 can be operated by a single operator. Actuators controls with USB2Dynamixel, measured data flow control with x-UMI, control algorithms processing and the real time changing view of FSRs and trunk oscillation are realized by user interface of control panel.

Figure 4.8 User interface of control panel for the biped robot RUBI-2.

CHAPTER FIVE
BIPED CONTROLLERS

5.1 Introduction

In this chapter, common online control methods, those are used in biped robots, are introduced. Real-time or precalculated walking pattern generation is needed to be compensated by online controllers, because the walking pattern cannot exactly satisfy the desired ZMP. Generally, the walking control method is based on switching strategies. Different online controllers are activated at the different stages of walk.

Such as damping controller was designed to eliminate the oscillation of the torso in the single support phase (Kim & Oh, 2004). The robot was simplified model as an inverted pendulum is oscillating around the ankle joint. The actual ankle joint angle due to compliance is improved by using the torque feedback of the force/toque sensor.

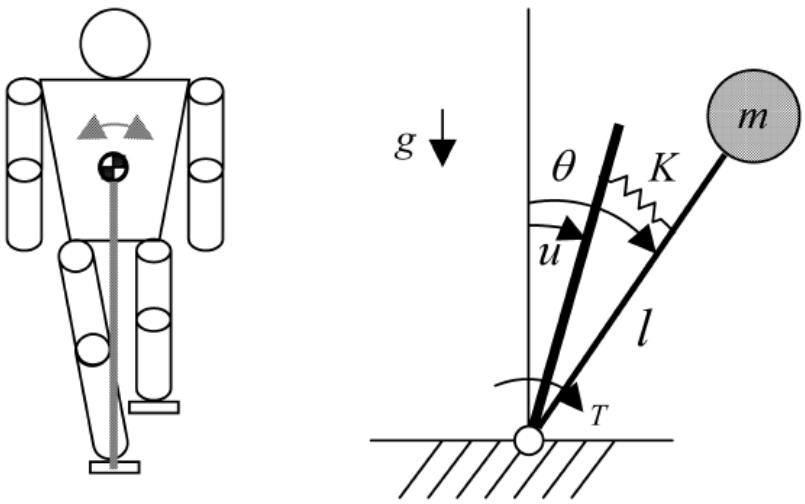

Figure 5.1 IPM model with compliant joint in the single support phase (Kim, Lee, & Ho, 2007).

Figure 5.1 shows the single support phase model for IPM, where T is the measured torque, g is the gravitational acceleration, L is the distance from the ground to the center of the mass, m is the total point mass, u is the reference joint angle, θ is

the actual joint angle due to the compliance and K is the stiffness of the leg. The equation of motion and the damping control law are given as follows:

$$T = mgl\theta - mgl^2\ddot{\theta} = K(\theta - u) \tag{5.1}$$
$$u_c = u - k_d\dot{\theta} \tag{5.2}$$

where k_d is the damping control gain and u_c is the compensated joint angle.

ZMP Compensator also works in single support phase (Kim, Park, & Oh, 2006). It helps the damping controller to maintain stable walk. The pelvis displacement is used as the input. ZMP compensator is designed by experimental frequency analysis and using pole placement method. The ZMP dynamics of the simple inverted pendulum model is given in equation 5.3.

$$Y_{ZMP} = Y_{pelvis} - \frac{l}{g}\ddot{Y}_{pelvis} \tag{5.3}$$

where Y_{pelvis} is the lateral displacement of the pelvis, l is the distance from the ground to the center of mass, g is the gravitational acceleration and Y_{ZMP} is the y-direction ZMP shown in Figure 5.2. The ZMP error can be compensated for as follows:

$$u_{comp} = K(ZMP - ZMP_{ref}) \tag{5.4}$$

where u_{comp} is the compensator displacement of the pelvis on the transverse plane and ZMP_{ref} is the reference ZMP.

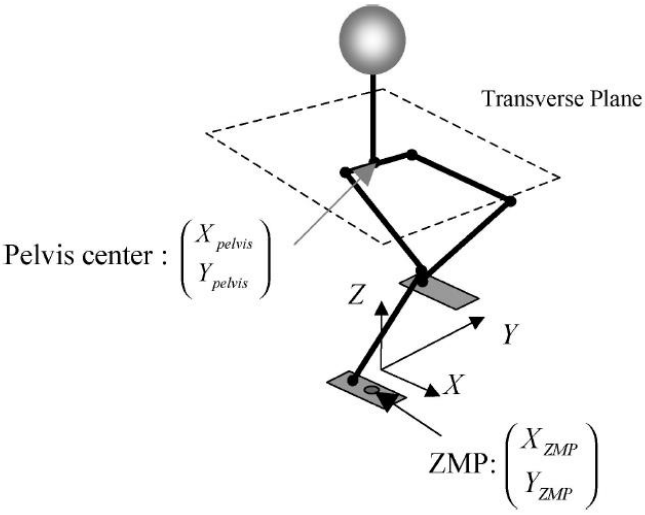

Figure 5.2 Motion of the pelvis for the ZMP compensation (Kim, Lee, et al., 2007).

The landing controllers are needed to be activated a short time when the foot touches the ground. The landing orientation controller is designed for a smooth landing if the ground is inclined (Kim, Lee, et al., 2007). For soft landing, the ankle joint moves like spring-damper system by using the torque feedback of the force/toque sensor (Figure 5.3). The control law of the landing control is given following equation.

$$u_c(s) = u(s) + \frac{T(s)}{Cs+K} \tag{5.5}$$

where T is the measured torque, C is damping coefficient, K is the stiffness, u is the reference angle of ankle and u_c is compensated reference angle of ankle.

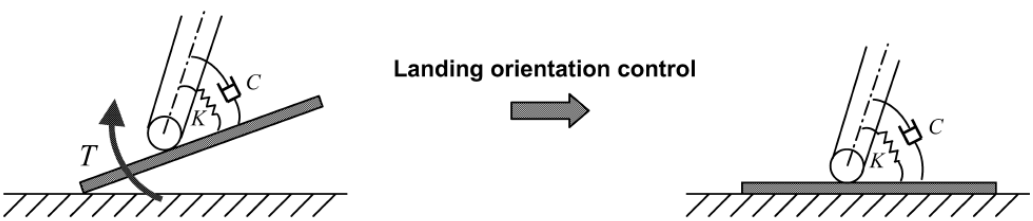

Figure 5.3 The landing orientation control (Kim, Lee, et al., 2007).

In this method, the landing shock absorber reduces the vertical forces which have occurred the foot touches the ground. It is assumed that a virtual spring-damper system is installed between ankle and hip joints. Controller uses a normal force as an input and can be absorbed through a rapid changing of the height of the hip joint. Equation 5.6 represents the control of the landing shock absorber as shown Figure 5.4.

$$z_c(s) = z(s) + \frac{F_z(s)}{ms^2+cs+k} \tag{5.6}$$

where F_z is the measured normal force, c is the damping coefficient, k is the stiffness, z is the reference pelvis height, z_c is the compensated reference pelvis height and m is the equivalent mass.

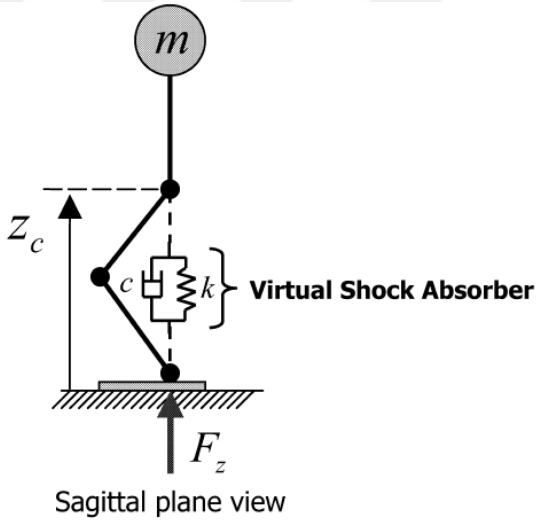

Figure 5.4 The landing shock absorber schematics in sagittal plane (Kim, Lee, et al., 2007).

Upright pose controller was designed to allow the robot to walk stably on a globally inclined floor (Kim, Park, & Oh, 2007). If the floor inclined, the walking of robot becomes unstable and the robot can be tilt over. The upright controller keeps the robot trunk upright by measuring the floor inclination. An inclinometer is placed to trunk and its data used as an input. Equation (5.7) represents the pitch control of the upright pose controller (Figure 5.5).

$$u'_{ankle\ pitch}(s) = u_{ankle\ pitch}(s) + (K_p + \frac{K_I}{s})\theta^{torso}_{err.p}(s) \tag{5.7}$$

where K_p and K_I are the proportional and integral gains, $u'_{ankle\ pitch}$ is the compensated ankle pitch angle, $\theta^{torso}_{err.p}$ is the torso pitch error and $u_{ankle\ pitch}$ is the prescribed ankle angle.

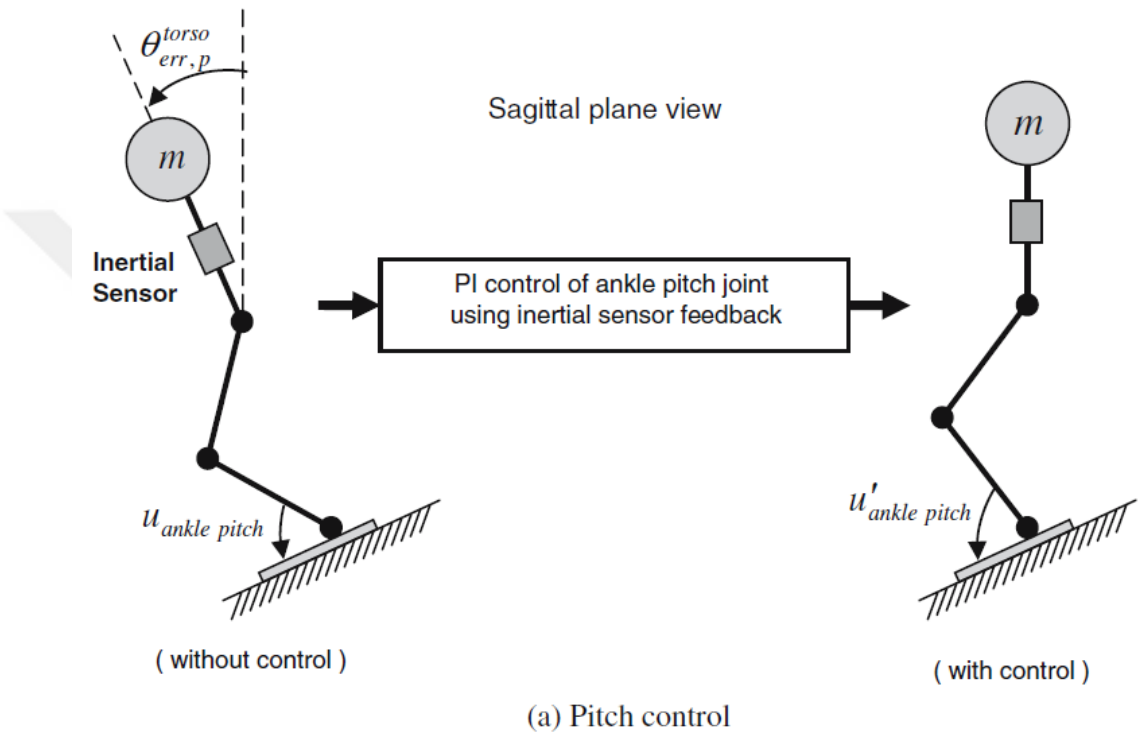

Figure 5.5 The upright pose control at sagittal plane (Kim, Park, et al., 2007).

The roll control parameters of the upright pose controller are calculated by following equations.

$$l'_L(s) = l_L(s) + (K_p + \frac{K_I}{s})\theta^{torso}_{err.r}(s) \tag{5.8}$$

$$l'_R(s) = l_R(s) - (K_p + \frac{K_I}{s})\theta^{torso}_{err.r}(s) \tag{5.9}$$

$$u'_{ankle\ roll} = u_{ankle\ roll} + \tan^{-1}\left(\frac{l'_R - l'_L}{Lateral\ distance\ between\ ankle\ joints}\right) \tag{5.10}$$

where K_p and K_I are the proportional and integral gains, $u'_{ankle\ roll}$ is the compensated ankle roll angle, $\theta^{torso}_{err.r}$ is the torso roll error, $u_{ankle\ roll}$ is the

prescribed ankle angle. l_R and l_L is the prescribed height of the right and left leg and l'_R and l'_L is the compensated height of the right and left leg, as shown in Figure 5.5.

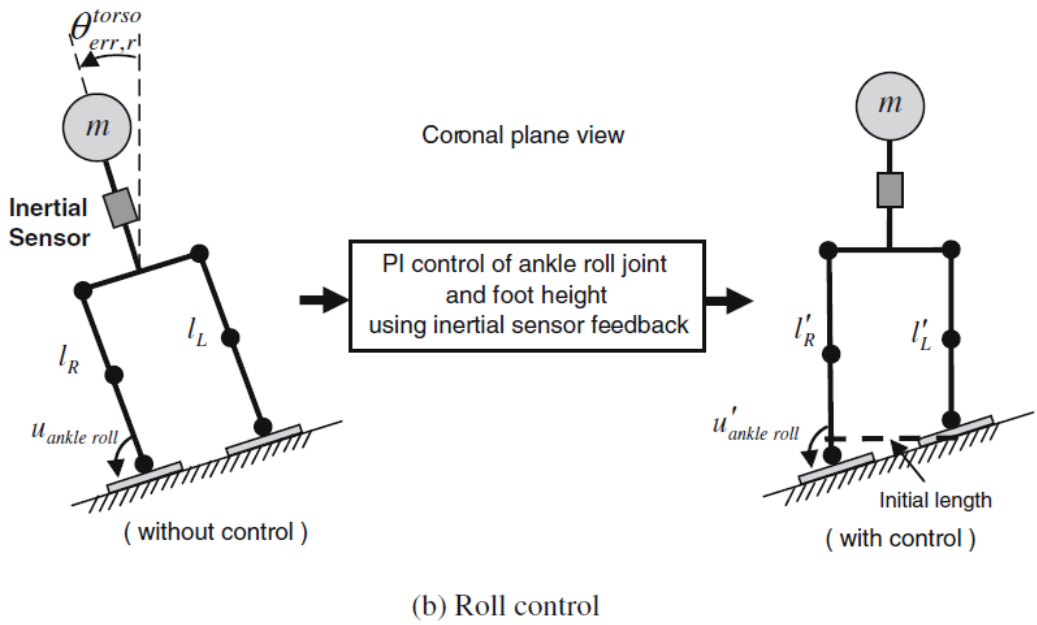

Figure 5.6 The upright pose control at frontal plane (J.-Y. Kim, Park, et al., 2007).

More advanced controllers are proposed for uneven and inclined floor (Kim, Park, et al., 2007). Landing angular momentum control, landing shock absorber, landing timing controller, landing position controller and vibration reduction controller are examples of these advanced controllers.

5.2 Design of Robot Controller

Design and implementation of robot controller depends strongly on sensor feedback and is limited to the sensor's performance. Also, considerable experimental fine tuning is required. In this thesis study, robot control strategy is proposed as shown in Figure 5.7. Three different type feedback sensors have been used on the robot control; Force sensors are under the feet, inertial measurement unit is located at the robot trunk and encoders integrated with motors are at the joints.

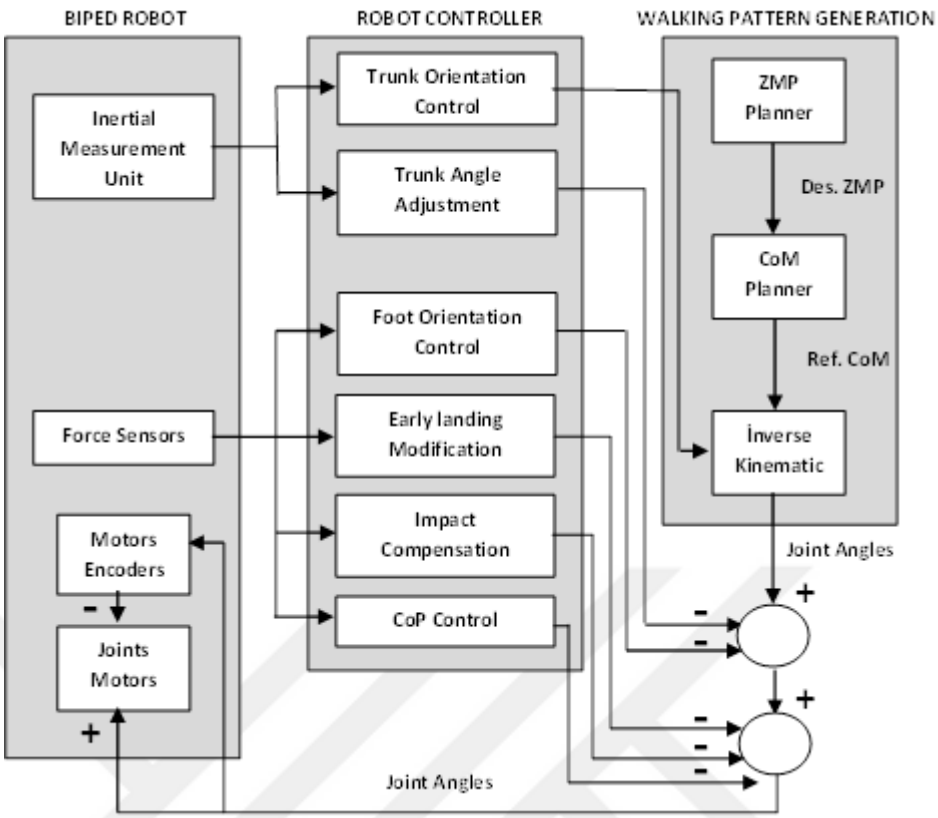

Figure 5.7 Proposed and implemented robot control strategy.

5.2.1 Joint Actuator PI Controller

Each joint actuator has own embedded PI controller which corrects joint position in 0,29° degree error. Figure 5.8 shows the relationship between output torque and the position of the motor. Punch, slope and margin values can be tuned up for each motor. When motor shaft reaches the goal position, maximum torque decreases with the compliance slope (A) and torque becomes zero at the compliance margin (B). Motor starts the motion by punch (E) value with the margin (C) and reaches the maximum torque following the compliance slope (D).

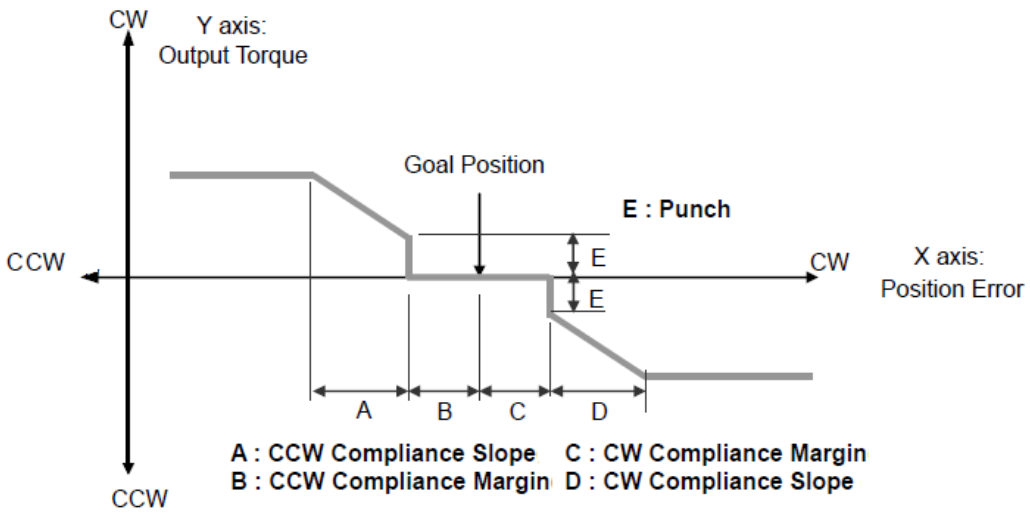

Figure 5.8 Motor position controls.

5.2.2 CoP Control

CoP controller was designed to maintain stable walking in the single support phase. In the Sections 2.3 and 2.4, CoP and ZMP were introduced. If the ZMP is within the convex hull of all contact points between the feet and the ground, a dynamically stable walking motion can be achieved. Also it is introduced that ZMP ≡ CoP when robot walking dynamically stable (Goswami, 1999; Vukobratovic & Borovac, 2004). CoP points position X_{CoP} and Y_{CoP} are easily found with following equations,

$$x_{CoP} = \frac{\sum f_i * x_i}{\sum f_i} \tag{5.11}$$

$$y_{CoP} = \frac{\sum f_i * y_i}{\sum f_i} \tag{5.12}$$

where x_i and y_i are the position for the force sensor according to foot reference coordinate, shown in Figure 5.9 and f_i is a normal force measured from force sensor. If the Cop point exits through the Stabil regions of foot area in x and y directions, the controller compensates the ankle roll and pitch angle by equations 5.13 and 5.14.

$$u'_{ankle\ pitch}(s) = u_{ankle\ pitch}(s) + (K_p + \frac{K_I}{s})x_{err}^{CoP}(s) \tag{5.13}$$

$$u'_{ankle\ roll}(s) = u_{ankle\ roll}(s) + (K_p + \frac{K_I}{s})y_{err}^{CoP}(s) \tag{5.14}$$

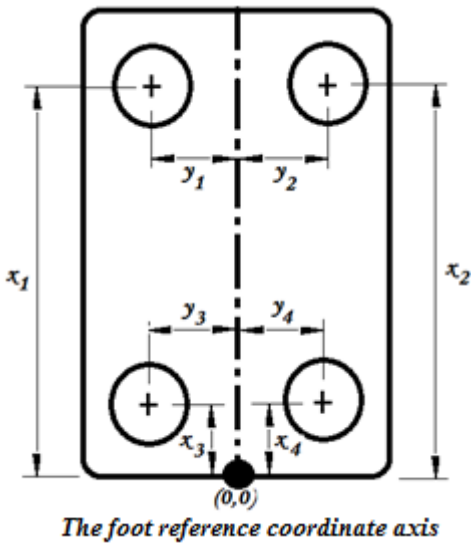

Figure 5.9 The foot reference coordinate axis and location of force sensors.

5.2.3 Trunk Angle Adjustment Control

The controller is designed to keep the robot trunk upright. Also, the controller compensates the ankle joint to prevent tilt over in single support phase. A roll and pitch angles measurement of the inertial measurement units are used as an input. Controller equations are given in 5.15 and 5.16.

$$u'_{ankle\ pitch}(s) = u_{ankle\ pitch}(s) + (K_p + \frac{K_I}{s})\theta^{trunk}_{err.pitch}(s) \tag{5.15}$$

$$u'_{ankle\ roll}(s) = u_{ankle\ roll}(s) + (K_p + \frac{K_I}{s})\theta^{trunk}_{err.roll}(s) \tag{5.16}$$

5.2.4 Foot Orientation Control

Foot orientation control provides the full foot contact of the ground at walking preparation phase and can be used for a smooth landing if the ground is inclined. Force sensors are used as input. Total normal force measured from force sensors, like a CoP controller, can be positioned to target area. Control schema of this controller is represented in Section 7.1.

5.2.5 Early Landing Modification

If the robot is tilted inside, the swing foot may land before the estimated landing time. Generally, the robot does not fall down due to early landing. However, it is needed to stop the walking pattern flow at the swing foot until the robot reach the right position. Normal forces are used inputs as measured from force sensors.

5.2.6 Impact Compensation

The impact compensation is designed to reduce the vertical forces when the foot touches the ground. Controller behaves like a virtual spring-damper system is installed between ankle and hip joints. A normal force uses as an input and can be absorbed through a rapid chancing of the height of the hip joint by equation 5.17.

$$z_c(s) = z(s) + \frac{F_z(s)}{ms^2+cs+k} \tag{5.17}$$

5.2.7 Trunk Orientation Control

Trunk orientation control keeps the robot trunk upright of the ground at walking preparation phase. A posture position of the robot is modified before the invers kinematics, if the ground is globally inclined. The inertial measurement units are used as input to compensate the ankle joint angle. Control schema of this controller is represented in Section 7.2.

CHAPTER SIX
SIMULATION

After the generations of the walking trajectories, it is needed to determine the parameters of robot joint angles. It is called as inverse kinematics that transforms the walking gait into joint actuator angle data for the robot by use of kinematic equations. The equations of the dynamics and kinematics of the biped robot mechanisms are needed to solve for finding the required actuator characteristics. Different mathematics models and simulation programs are studied to solve this problem by some researchers (Erbatur & Kurt, 2009; Fujimoto & Kawamura, 1998; Qiang, Nakamura, Arai, & Tanie, 2000; Qiang et al., 2001). In this thesis, the biped robot motion is simulated by CosmosMotion that is the part of SolidWorks. The necessary joint actuators parameters like a joint projection angles and joint torques are calculated by simulation.

The walking pattern generation foundations of the biped robot are explained in the chapter three. Depends on walking equations, assumed constrains and the design parameters of the biped robot, RUBI-2 walking was simulated. In this chapter, simulation studies done with two well-known methods given in chapter three.

6.1 Walking Pattern Generation by The Foot Parameters

The walking pattern generation by the foot parameters is explained in Section 3.1. There are some assumptions to simplify robot dynamics. In this thesis work, the walking cycle of biped robot is analyzed on the sagittal and transverse plane. It is assumed that the swing foot is moving parallel the ground. As a result of this, the angle of the foot $\theta_a(t) = 0$ when biped robot is walking. Also, it is assumed that the biped robot's legs move always parallel to each other. If robot moves on the flat surface, $q_{gs}(k) = q_{ge}(k) = 0$ and $h_{gs}(k) = h_{ge}(k) = 0$.

The walking trajectories should be continuous at both first and second order derivatives to obtain smooth walking pattern. This guarantees the smoothness of

velocities and accelerations. To reach the continuous walking trajectories, using third-order interpolation is the best way (Qiang et al., 2001; Zhe et al., 2003). In this thesis, cubic spline interpolation was used for walking trajectory planning.

The swing foot trajectories are easily generated by equation (3.2) and (3.3). The parameters used in the foot parameter method are given as; the period of walking step was T_c = 0.9 s/step, the length of step was D_s = 110 mm/step, the interval of the double support phase was T_d = 0,15 s, the position of the highest point of the swing foot ankle were L_{ao} = 50 mm, H_{ao} = 100 mm and the time of the highest point of the swing foot ankle T_m = 0,5 s.

Figure 6.1 shows the foot trajectory along x-axis for the foot parameter method according to equation (3.2).

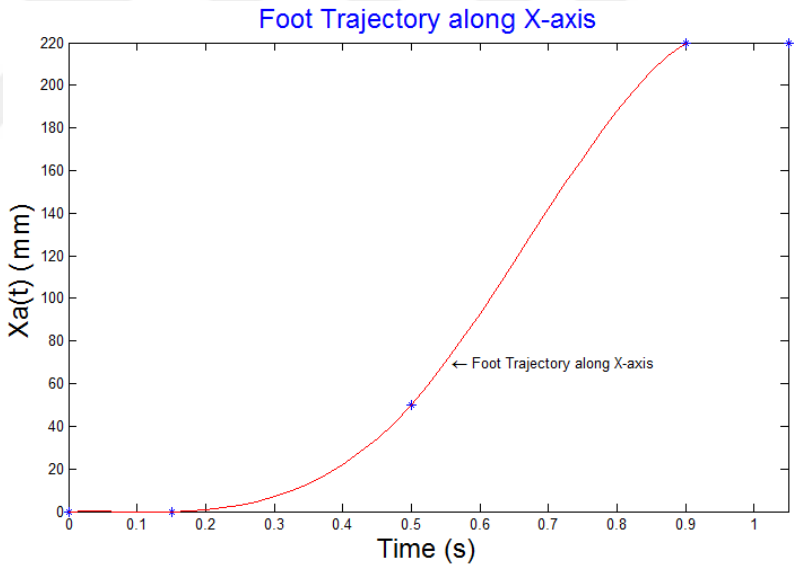

Figure 6.1 The foot trajectory along x-axis for the foot parameter method.

Figure 6.2 shows the foot trajectory along z-axis for the foot parameter method according to equation (3.3).

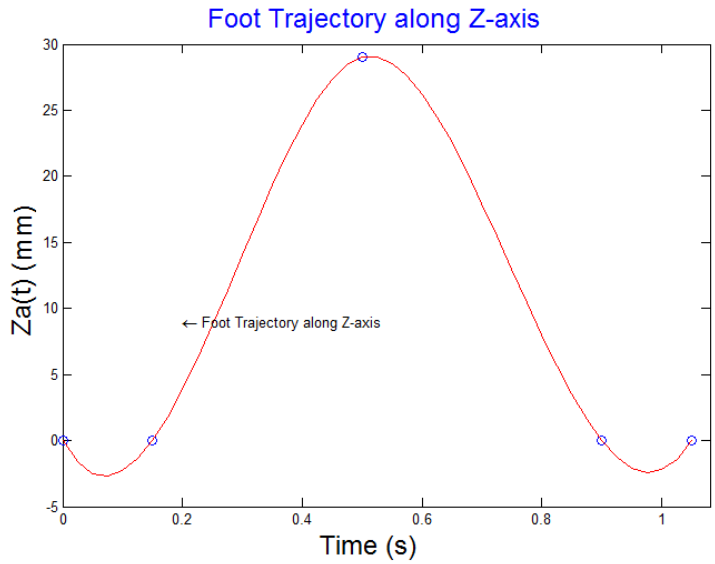

Figure 6.2 The foot trajectory along z-axis for the foot parameter method.

The hip trajectories are generated by equation (3.5) and (3.6). Where, distances from the hip to the ankle of the support foot at the start and end of the single support phase were x_{sd} = 45 cm and x_{ed} = 45 cm. Also the robot hip moved between $H_{h\min}$ = 454 cm and $H_{h\max}$ = 464 cm.

Figure 6.3 shows the hip trajectory along x-axis for the foot parameter method according to equation (3.4).

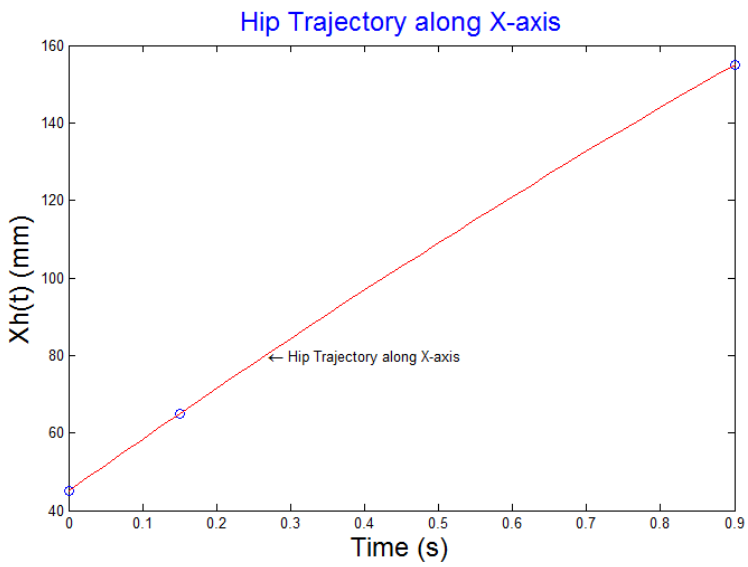

Figure 6.3 The hip trajectory along x-axis for the foot parameter method.

Figure 6.4 shows the hip trajectory along z-axis for the foot parameter method according to equation (3.5).

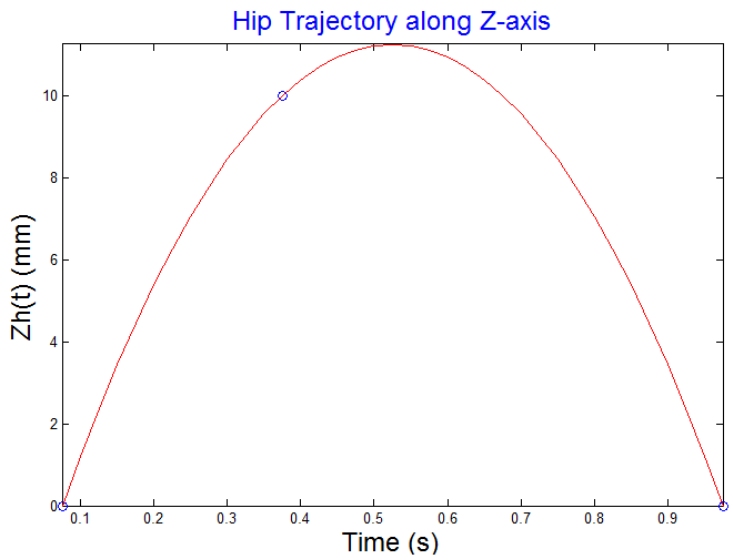

Figure 6.4 The hip trajectory along z-axis for the foot parameter method.

Although, the foot only moves at the sagittal plane, the hip moves on the sagittal and transverse plane. At the transverse plane, it is assumed that hip trajectory along y-axis is generated by harmonic spline curve, shown in Figure 6.5.

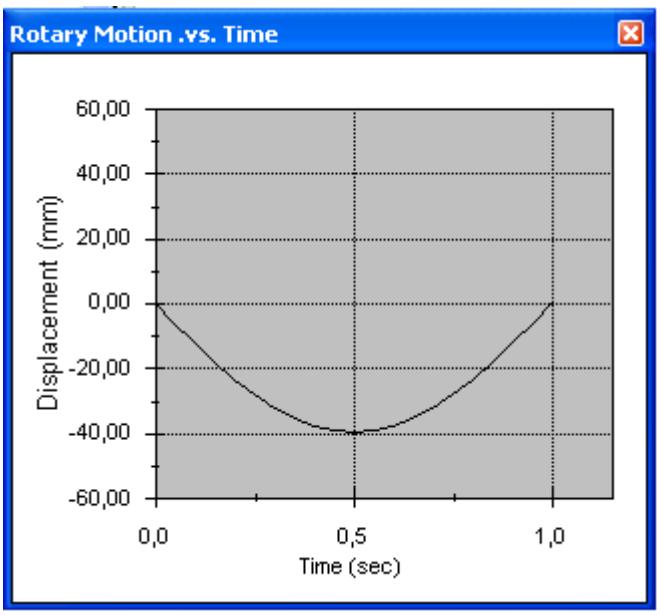

Figure 6.5 The hip trajectory along y-axis for the foot parameter method.

The foot and hip trajectory were used as input for simulation. To generate one complete walking cycle, two simple steps were simulated. Figure 6.6 is snapshots of walking simulation for the foot parameter method.

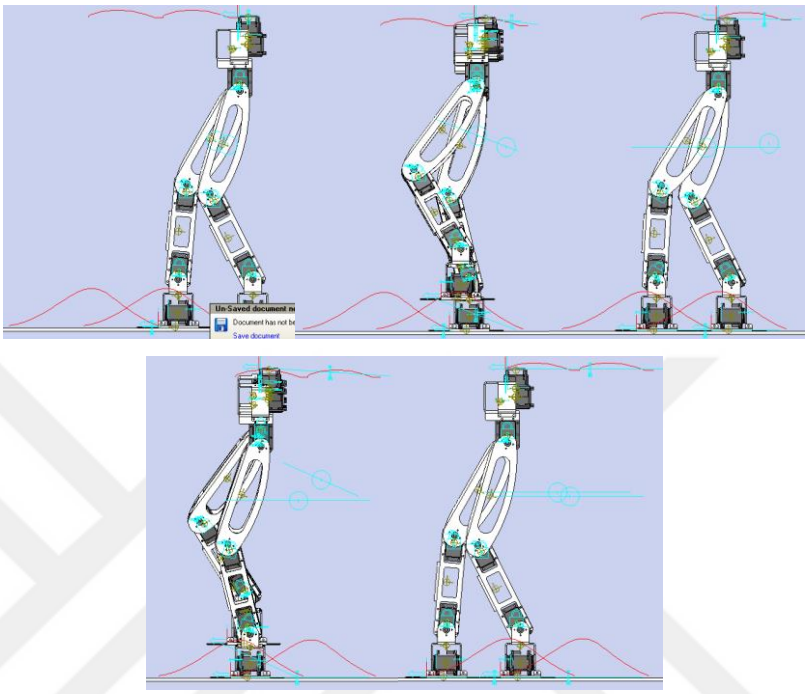

Figure 6.6 Walking simulation snapshots for the foot parameter method.

After the simulation, all joint angle and torque changes were achieved as shown in Figure 6.7 and Figure 6.8. As results, the maximum angle change is shown in Table 6.2 at the knee joint with 46 degrees and the maximum torque was approximately 110 Nmm (1.1 kgcm).

Table 6.1 Joint angle changes for walking trajectories by foot parameter method.

Joints	**Planes**	**Angle Changes (Degree)**	
		Left Leg	**Right Leg**
Hip	Frontal	-9 to 8	-9 to 8
Hip	Transverse	0	0
Hip	Sagittal	-1 to 21	-16 to 6
Knee	Sagittal	-14 to 28	0 to 46
Ankle	Sagittal	-30 to 8	0 to 40
Ankle	Frontal	-9 to 8	-9 to 8

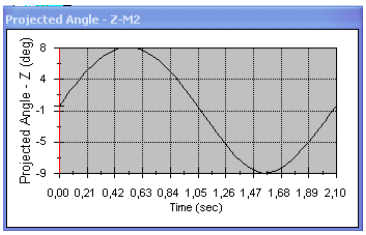

a) Right ankle joint angles at frontal plane.

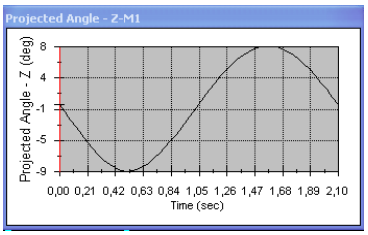

b) Left ankle joint angles at frontal plane.

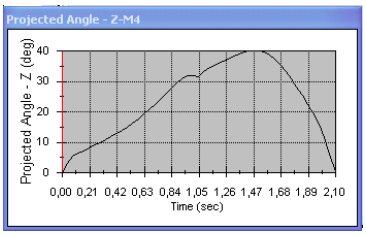

c) Right ankle joint angles at sagittal plane.

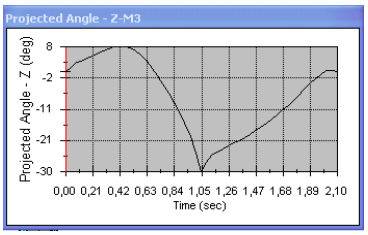

d) Left ankle joint angles at sagittal plane.

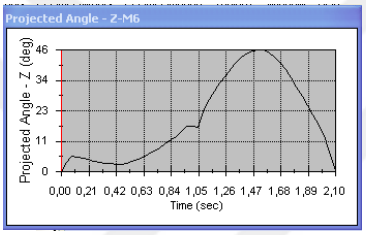

e) Right knee joint angles at sagittal plane.

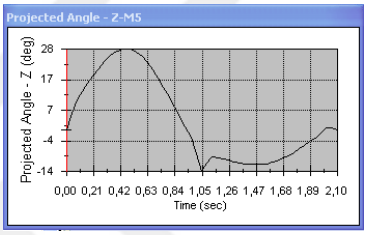

f) Left knee joint angles at sagittal plane.

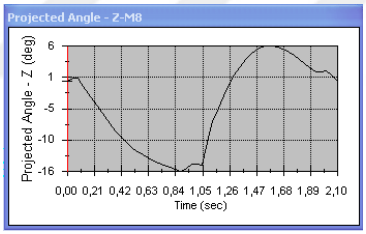

g) Right hip joint angles at sagittal plane.

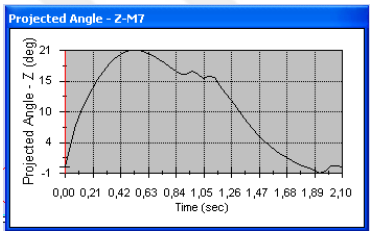

h) Left hip joint angles at sagittal plane.

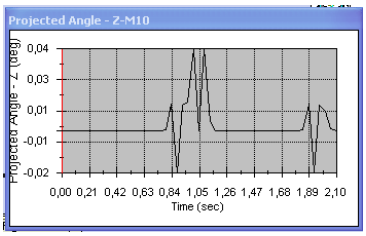

i) Right hip joint angles at transverse plane.

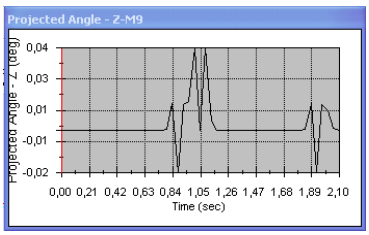

j) Left hip joint angles at transverse plane.

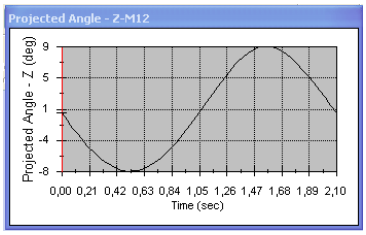

k) Right hip joint angles at frontal plane.

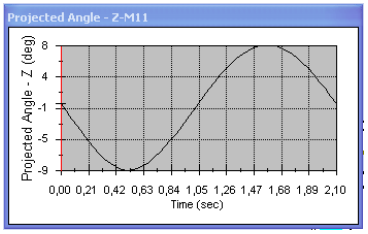

l) Left hip joint angles at frontal plane.

Figure 6.7 Joint angle changes for one single step by the foot parameters simulation.

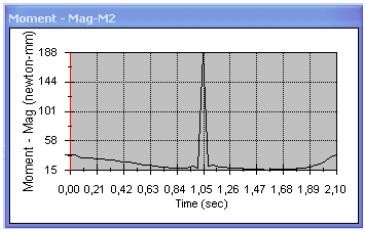

a) Right ankle joint torques at frontal plane.

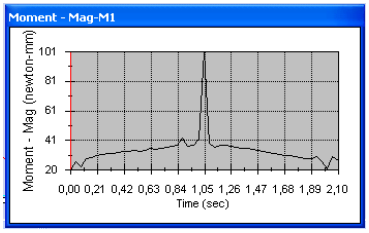

b) Left ankle joint torques at frontal plane.

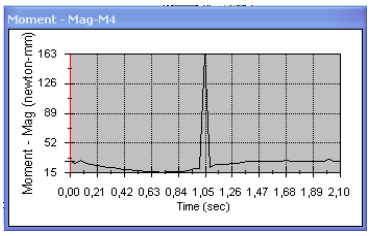

c) Right ankle joint torques at sagittal plane.

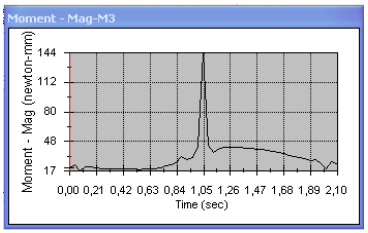

d) Left ankle joint torques at sagittal plane.

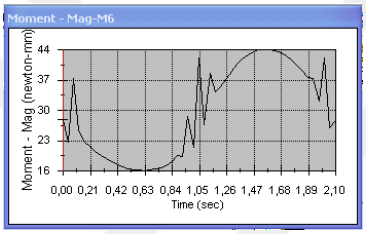

e) Right knee joint torques at sagittal plane.

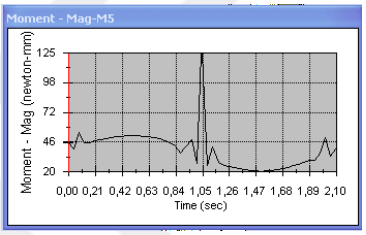

f) Left knee joint torques at sagittal plane.

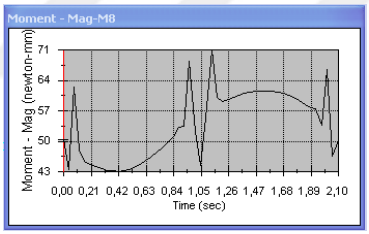

g) Right hip joint torques at sagittal plane.

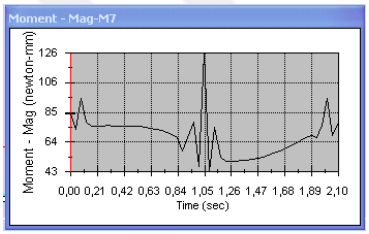

h) Left hip joint torques at sagittal plane.

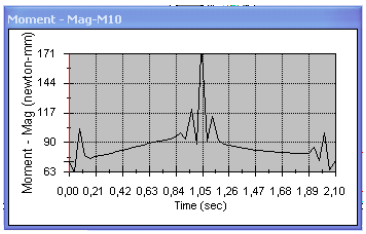

i) Right hip joint torques at transverse plane.

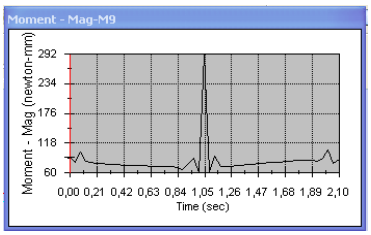

j) Left hip joint torques at transverse plane.

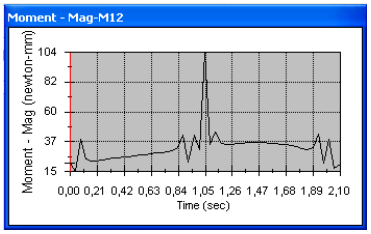

k) Right hip joint torques at frontal plane.

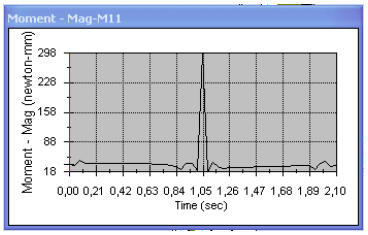

l) Left hip joint torques at frontal plane.

Figure 6.8 Joint torque changes for one single step by the foot parameters simulation.

6.2 Walking Pattern Generation by Linear Inverted Pendulum Model

This walking pattern generation method interested in finding the CoM trajectories are explained in Section 3.2. The approximate solutions of CoM trajectories are generated with T = 1,05 s, n=12, A = 65 mm, B = 110 mm and w_n^2 = 21.36 (c_z = 459 mm and g = 9,81 m/s) by equation (3.26) and (3.29).

Figure 6.9 and 6.10 show the reference CoM trajectories with the reference ZMP and Fourier approximation reference ZMP.

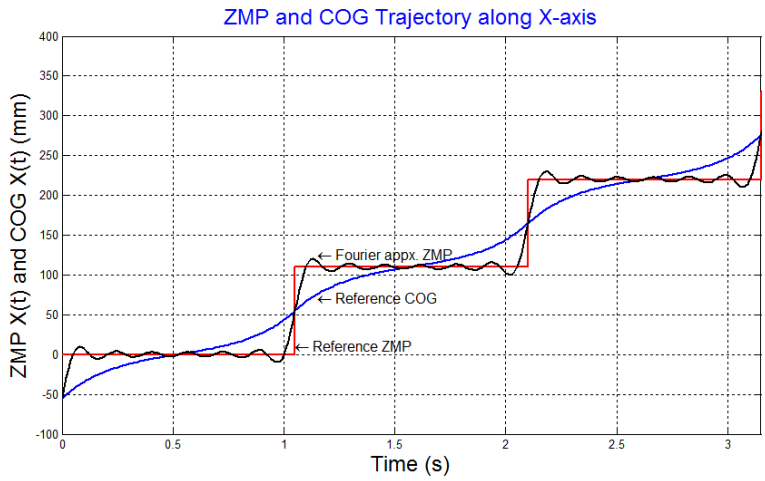

Figure 6.9 The reference CoM trajectories c_x^{ref} with Reference ZMP p_x and Fourier approximation reference ZMP p_x^{ref} for n = 12.

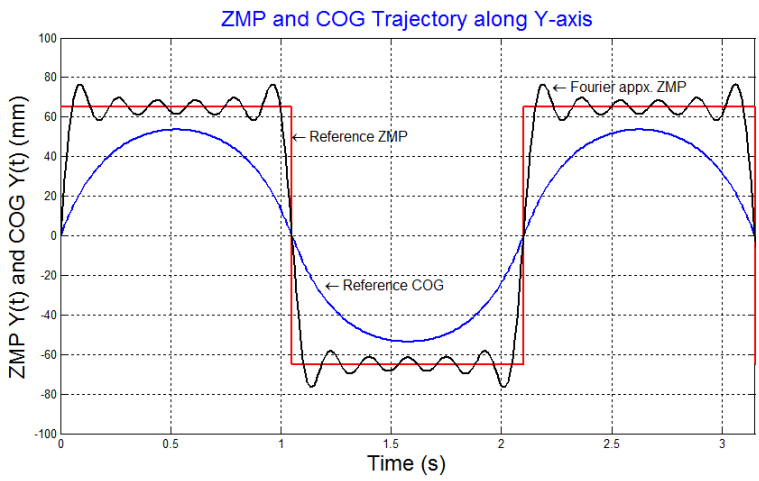

Figure 6.10 The reference CoM trajectories c_y^{ref} with Reference ZMP p_y and Fourier approximation reference ZMP p_y^{ref} for n = 12.

The swing foot trajectory is explained in 6.1 used as the foot trajectory in LIPM simulation. Figure 6.11 shows the foot trajectory along x-axis for LIPM according to equation (3.2).

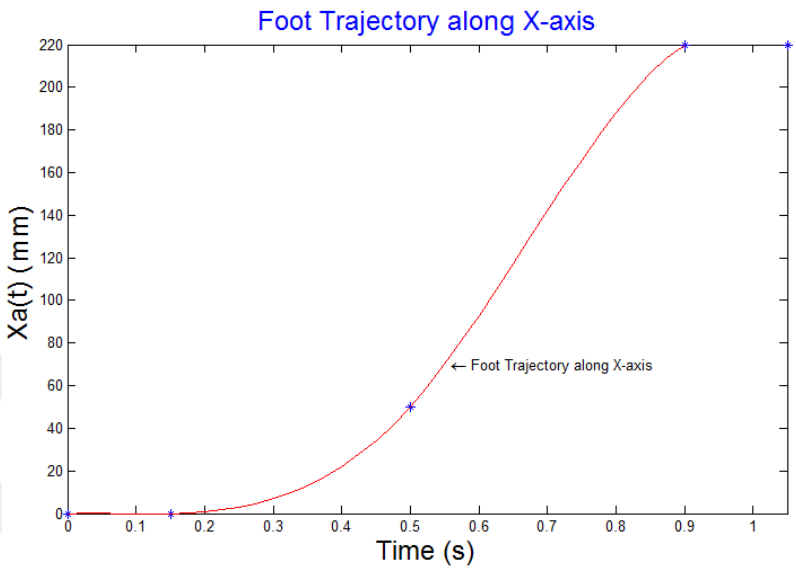

Figure 6.11 The foot trajectory along x-axis for LIPM.

Figure 6.12 shows the foot trajectory along z-axis for LIPM according to equation (3.3).

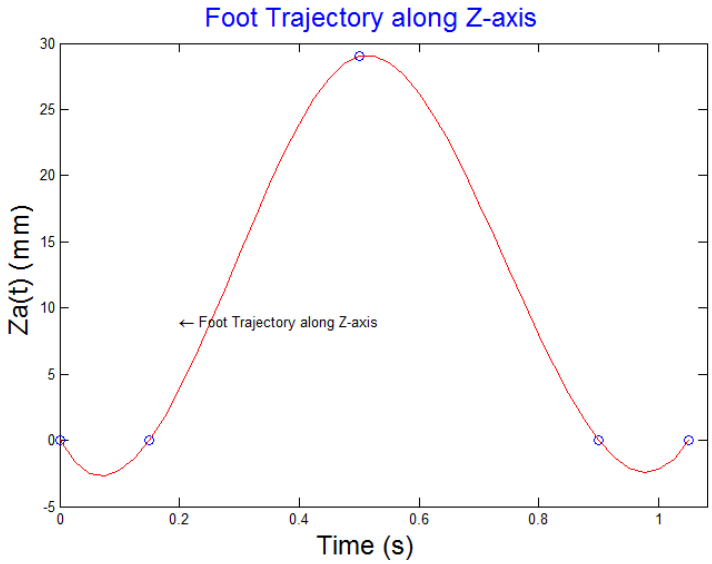

Figure 6.12 The foot trajectory along z-axis for LIPM.

CoM trajectory and the foot trajectory were used as input for simulation. Figure 6.13 is snapshots of one complete walking cycle simulation for LIPM.

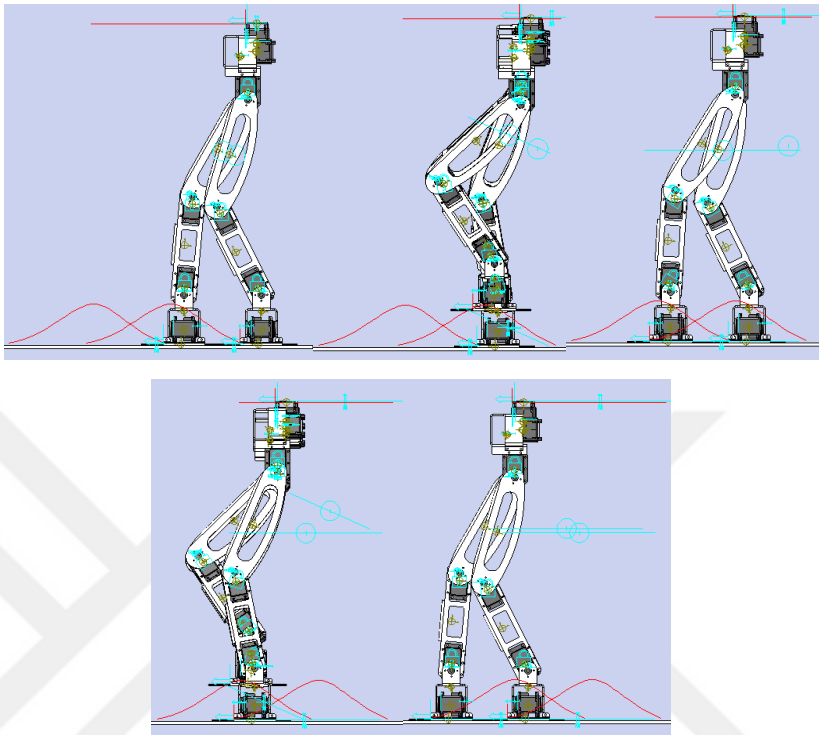

Figure 6.13 Walking simulation snapshots for LIPM.

After the simulation, all joint angle and torque changes were achieved as shown in Figure 6.14 and Figure 6.15. As results, the maximum angle change is shown in Table 6.2 at the knee joint with 58 degrees and the maximum torque was approximately 110 Nmm (1.1 kgcm).

Table 6.2 Joint angle changes for walking trajectories by LIPM.

Joints	**Planes**	**Angle Changes (Degree)**	
		Left Leg	**Right Leg**
Hip	Frontal	-8 to 9	-8 to 9
Hip	Transverse	0	0
Hip	Sagittal	-15 to 16	0 to -30
Knee	Sagittal	-14 to 40	0 to 58
Ankle	Sagittal	-30 to 13	0 to 45
Ankle	Frontal	-8 to 9	-8 to 9

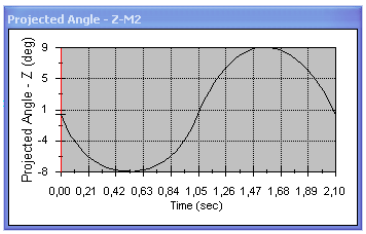

a) Right ankle joint angles at frontal plane.

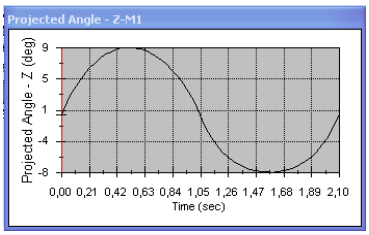

b) Left ankle joint angles at frontal plane.

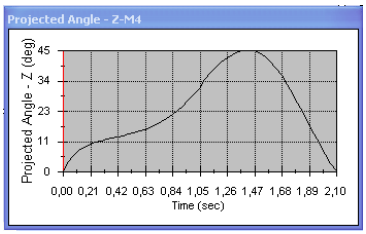

c) Right ankle joint angles at sagittal plane.

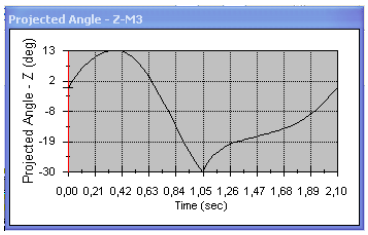

d) Left ankle joint angles at sagittal plane.

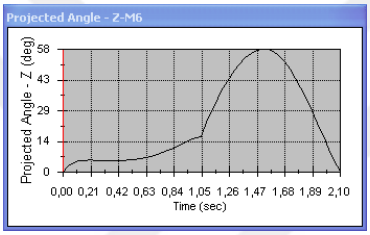

e) Right knee joint angles at sagittal plane.

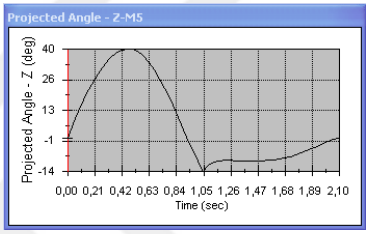

f) Left knee joint angles at sagittal plane.

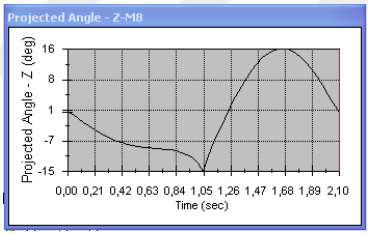

g) Right hip joint angles at sagittal plane.

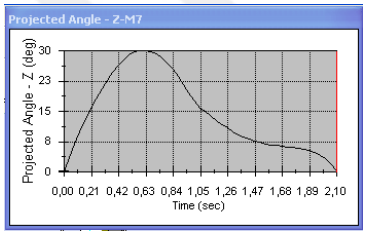

h) Left hip joint angles at sagittal plane.

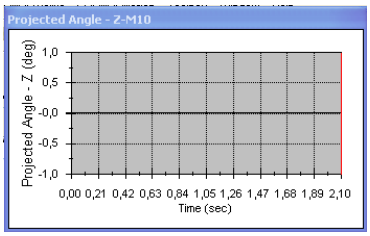

i) Right hip joint angles at transverse plane.

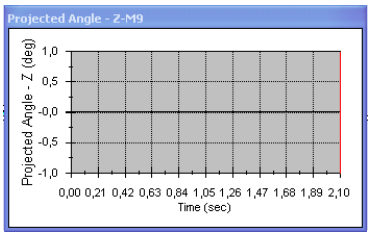

j) Left hip joint angles at transverse plane.

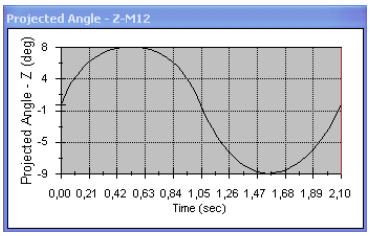

k) Right hip joint angles at frontal plane.

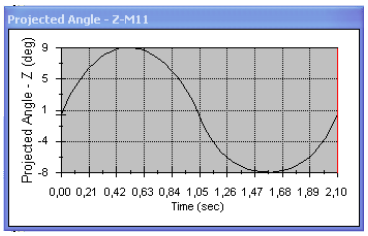

l) Left hip joint angles at frontal plane.

Figure 6.14 Joint angle changes for one single step by LIPM simulation.

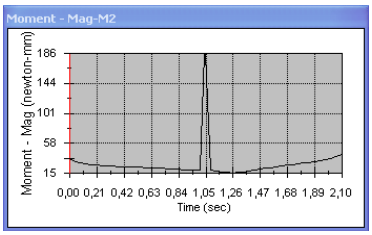

a) Right ankle joint torques at frontal plane.

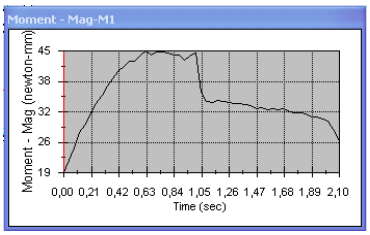

b) Left ankle joint torques at frontal plane.

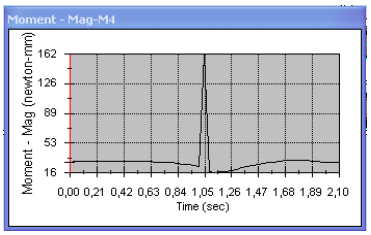

c) Right ankle joint torques at sagittal plane.

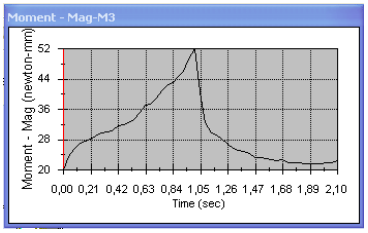

d) Left ankle joint torques at sagittal plane.

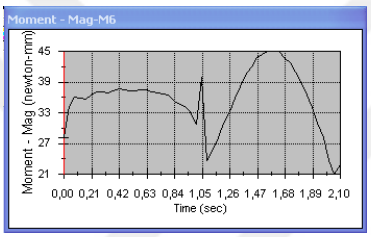

e) Right knee joint torques at sagittal plane.

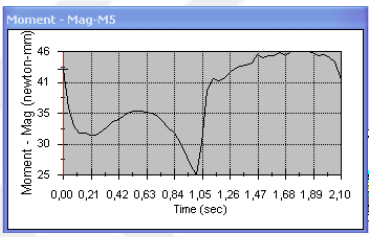

f) Left knee joint torques at sagittal plane.

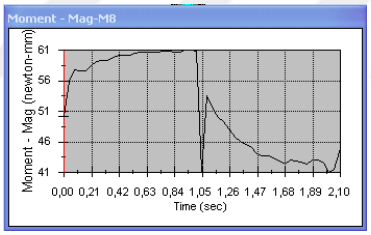

g) Right hip joint torques at sagittal plane.

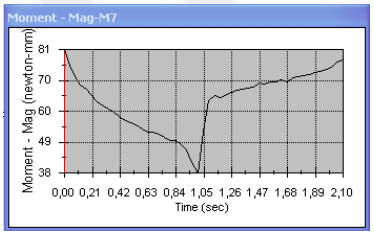

h) Left hip joint torques at sagittal plane.

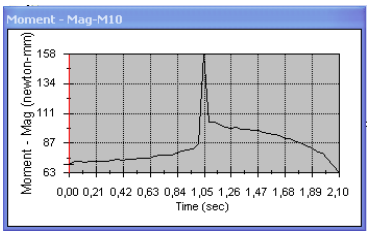

i) Right hip joint torques at transverse plane.

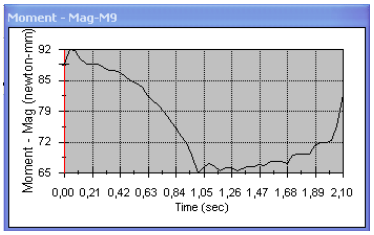

j) Left hip joint torques at transverse plane.

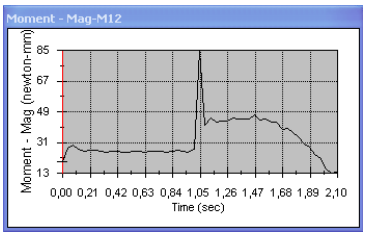

k) Right hip joint torques at frontal plane.

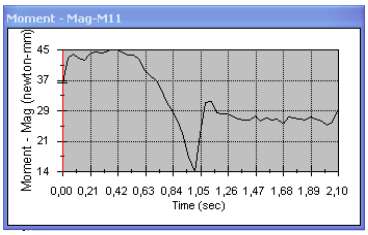

l) Left hip joint torques at frontal plane.

Figure 6.15 Joint torque changes for one single step by LIPM simulation.

Joint angles are obtained by LIPM and the foot parameters methods are compared in Figure 6.16

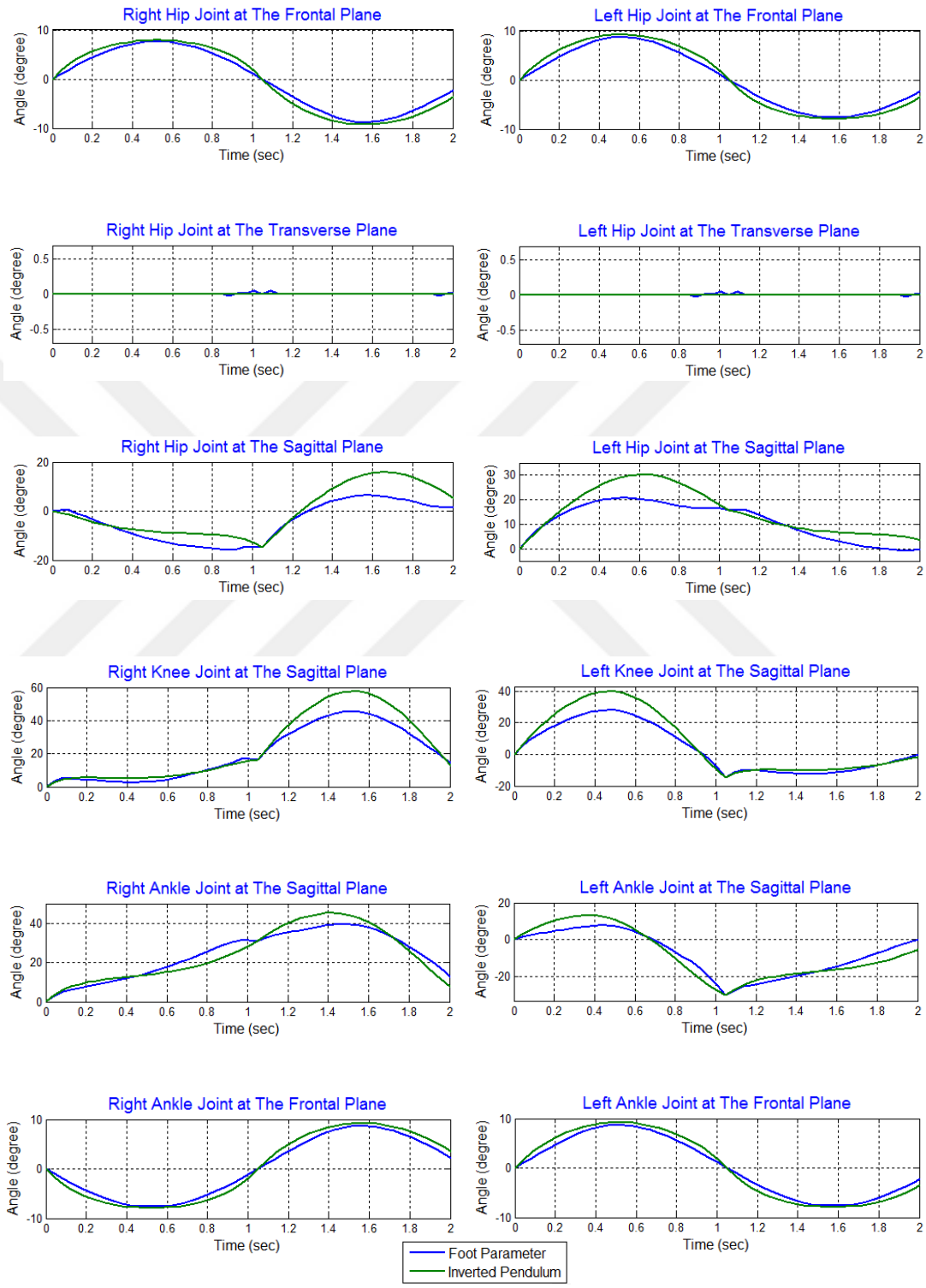

Figure 6.16 Comparison of Joint angles are obtained by LIPM and the foot parameters methods.

The simulation and experimental work results show that step size, swing foot position and hip height are hardy effect the robot balance. After the experimental fine tuning of these parameters, main walking trajectories are reached.

For main walking trajectories, the approximate solutions of CoM trajectories are generated with T = 1 s, n=12, A = 65 mm, B = 50 mm and $w_n^2 = 21.36$ ($c_z = 459$ mm and g = 9,81 m/s) for main walking trajectories. Figure 6.17 and 6.18 show the reference CoM trajectories with the reference ZMP and Fourier approximation reference ZMP.

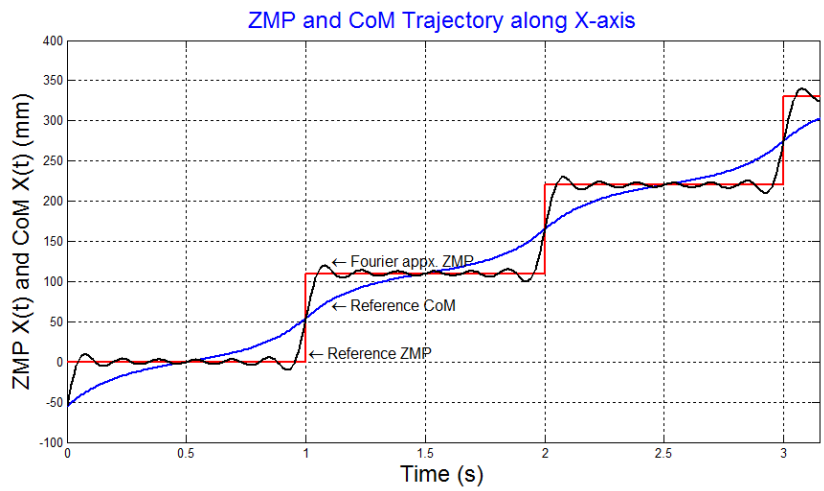

Figure 6.17 The reference CoM trajectories c_x^{ref} with Reference ZMP p_x and Fourier approximation reference ZMP p_x^{ref} for main walking trajectories.

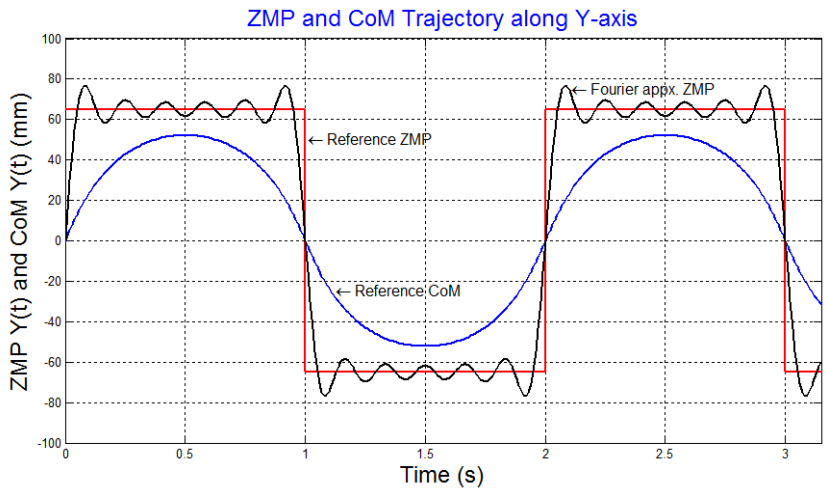

Figure 6.18 The reference CoM trajectories c_y^{ref} with Reference ZMP p_y and Fourier approximation reference ZMP p_y^{ref} for main walking trajectories.

The swing foot trajectories are generated by the period of walking step was T_c = 0.9 s/step, the length of step was D_s = 50 mm/step, the interval of the double support phase was T_d = 0,1 s, the position of the highest point of the swing foot ankle were L_{ao} = 50 mm, H_{ao} = 100 mm and the time of the highest point of the swing foot ankle T_m = 0,5 s. Figure 6.19 shows the foot trajectory along x-axis for main walking trajectories.

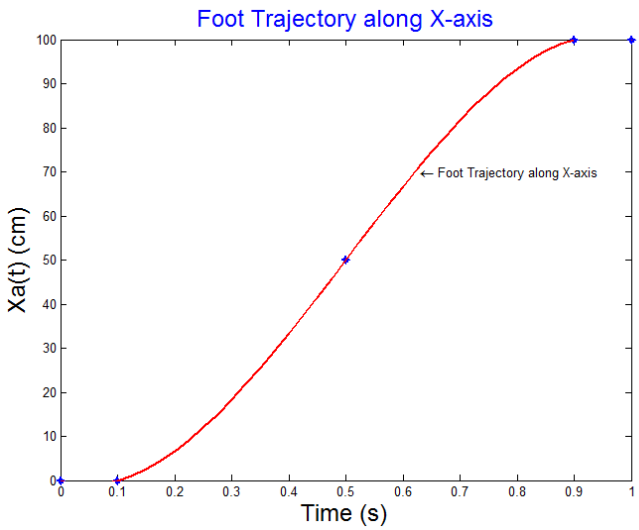

Figure 6.19 The foot trajectory along x-axis for main walking trajectories.

Figure 6.20 shows the foot trajectory along z-axis for main walking trajectories.

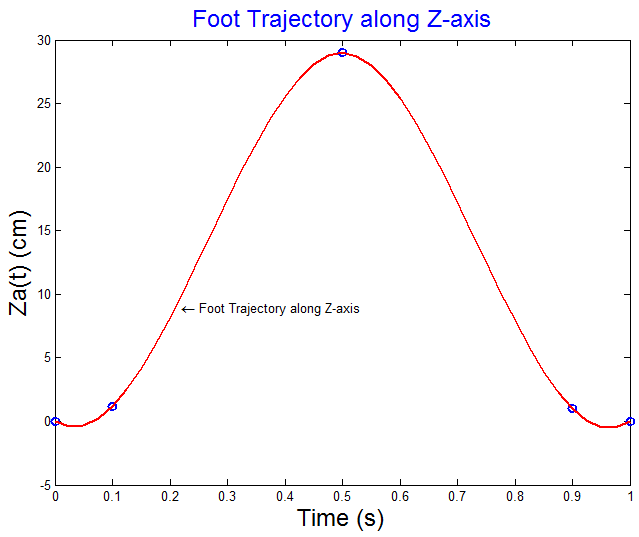

Figure 6.20 The foot trajectory along z-axis for main walking trajectories.

CoM trajectory and the foot trajectory were used as input for simulation. Figure 6.21 shows the snapshots of walking simulation for main walking trajectories.

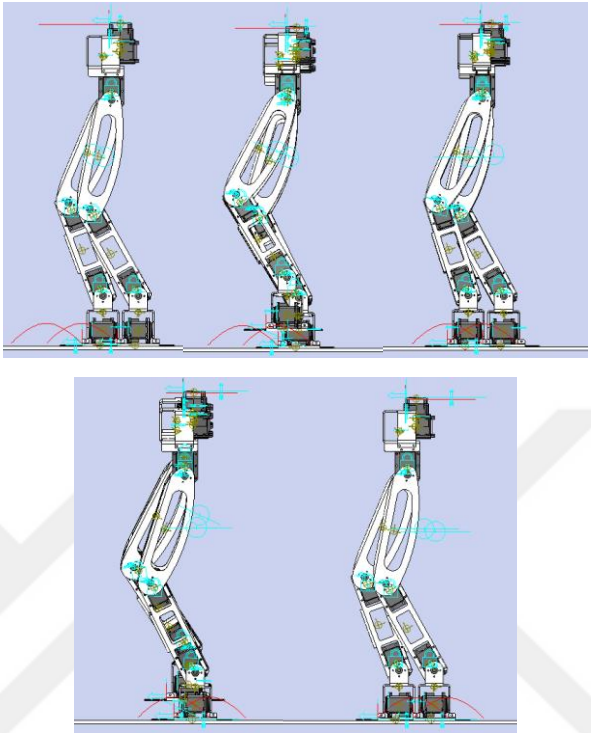

Figure 6.21 Walking simulation snapshots for main walking trajectories.

After the simulation, all joint angle and torque changes were achieved shown in Figure 6.22 and Figure 6.23. As results, the maximum angle change is shown in Table 6.3 at the knee joint with 25 degrees and the maximum torque was approximately 100 Nmm (1 kgcm).

Table 6.3 Joint angle changes for main walking trajectories.

Joints	**Planes**	**Angle Changes (Degree)**	
		Left Leg	**Right Leg**
Hip	Frontal	-8 to 8	-8 to 8
Hip	Transverse	0	0
Hip	Sagittal	-5 to 16	4 to 17
Knee	Sagittal	-17 to 8	-20 to 4
Ankle	Sagittal	-16 to 4	-7 to 12
Ankle	Frontal	-8 to 8	-8 to 8

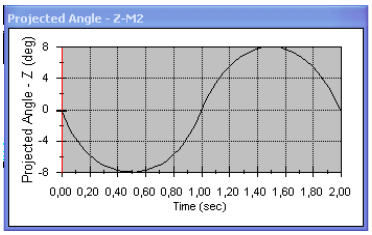

a) Right ankle joint angles at frontal plane.

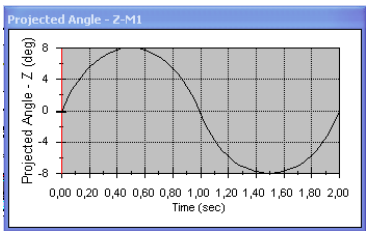

b) Left ankle joint angles at frontal plane.

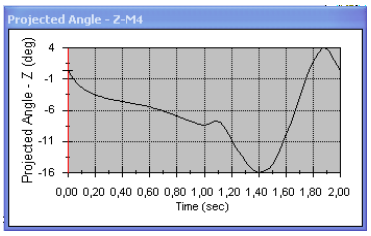

c) Right ankle joint angles at sagittal plane.

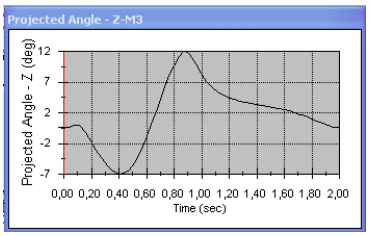

d) Left ankle joint angles at sagittal plane.

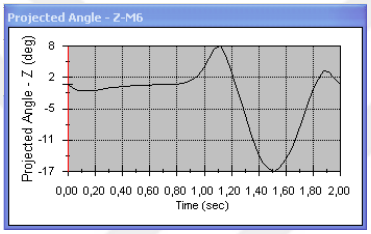

e) Right knee joint angles at sagittal plane.

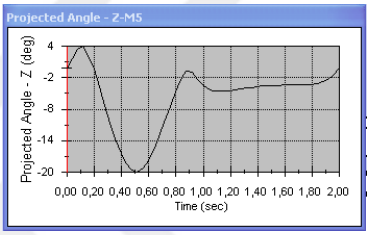

f) Left knee joint angles at sagittal plane.

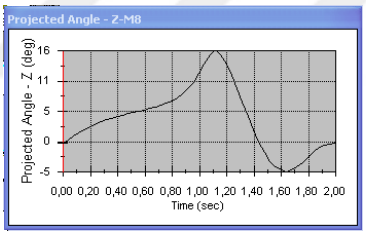

g) Right hip joint angles at sagittal plane.

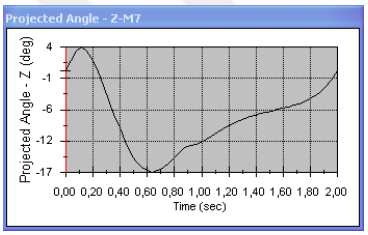

h) Left hip joint angles at sagittal plane.

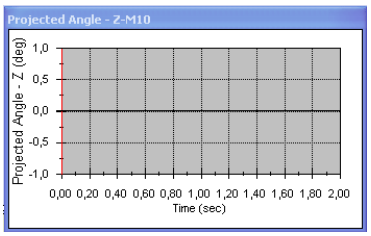

i) Right hip joint angles at transverse plane.

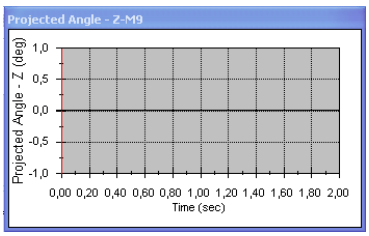

j) Left hip joint angles at transverse plane.

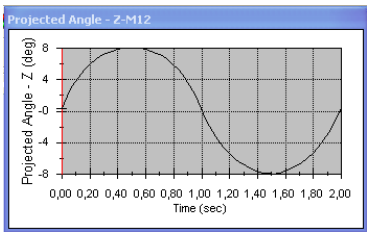

k) Right hip joint angles at frontal plane.

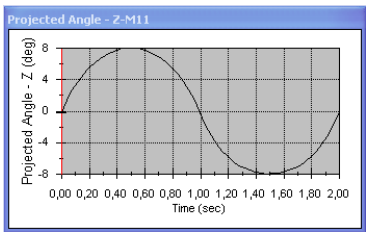

l) Left hip joint angles at frontal plane.

Figure 6.22 Joint angle changes for main step by LIPM simulation.

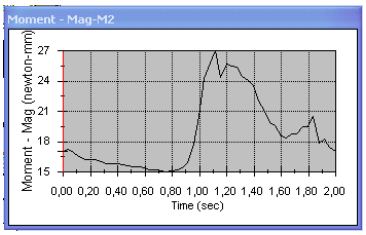

a) Right ankle joint torques at frontal plane.

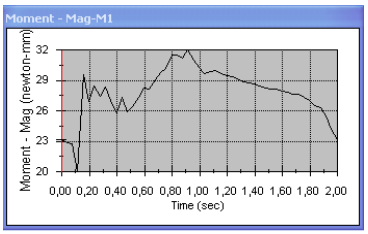

b) Left ankle joint torques at frontal plane.

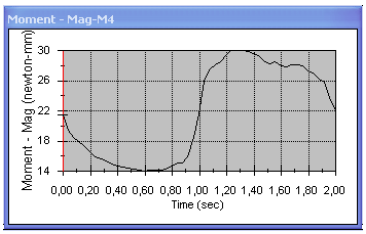

c) Right ankle joint torques at sagittal plane.

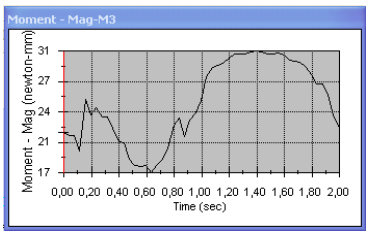

d) Left ankle joint torques at sagittal plane.

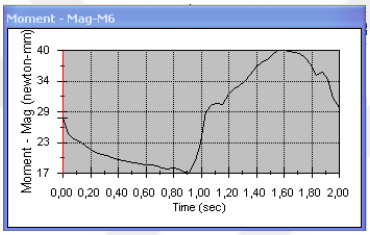

e) Right knee joint torques at sagittal plane.

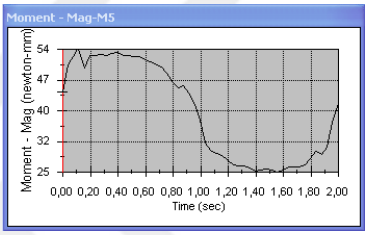

f) Left knee joint torques at sagittal plane.

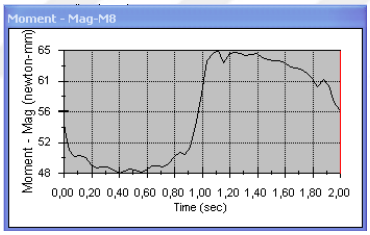

g) Right hip joint torques at sagittal plane.

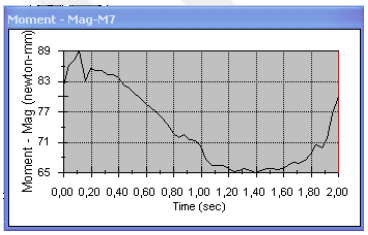

h) Left hip joint torques at sagittal plane.

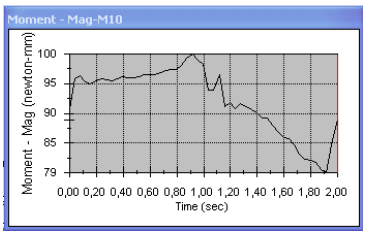

i) Right hip joint torques at transverse plane.

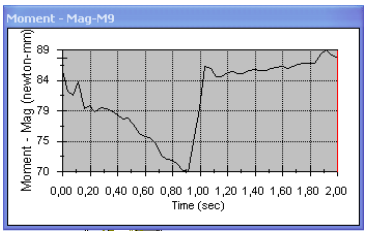

j) Left hip joint torques at transverse plane.

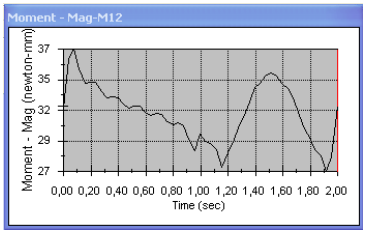

k) Right hip joint torques at frontal plane.

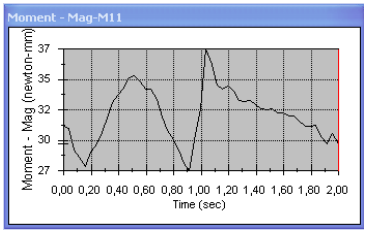

l) Left hip joint torques at frontal plane.

Figure 6.23 Joint torque changes for main step by LIPM simulation.

Except for one complete step generations and simulations, half-step and fixed height adjustment simulations were done. They are used as a transition step to pass from upright posture to walking position when walking beginning and from walking positions to upright posture when walking ending. This operation is realized by reorganizing main walking trajectory.

CHAPTER SEVEN
EXPERIMENTAL RESULTS

The proposed walking pattern generations and control methods were implemented on the biped robot RUBI-2.

7.1 Foot Orientation Experiments

Foot orientation control provides the full foot contact of the ground at walking preparation phase. It also provides the balance of the force distribution between feet.

In this experiment, force data acquired from foot force sensors are processed by filter. Filter process the differences of force and gives the related joint a correction. Matlab Simulink filters of roll and pitch position are shown in Figure 7.1 and 7.2.

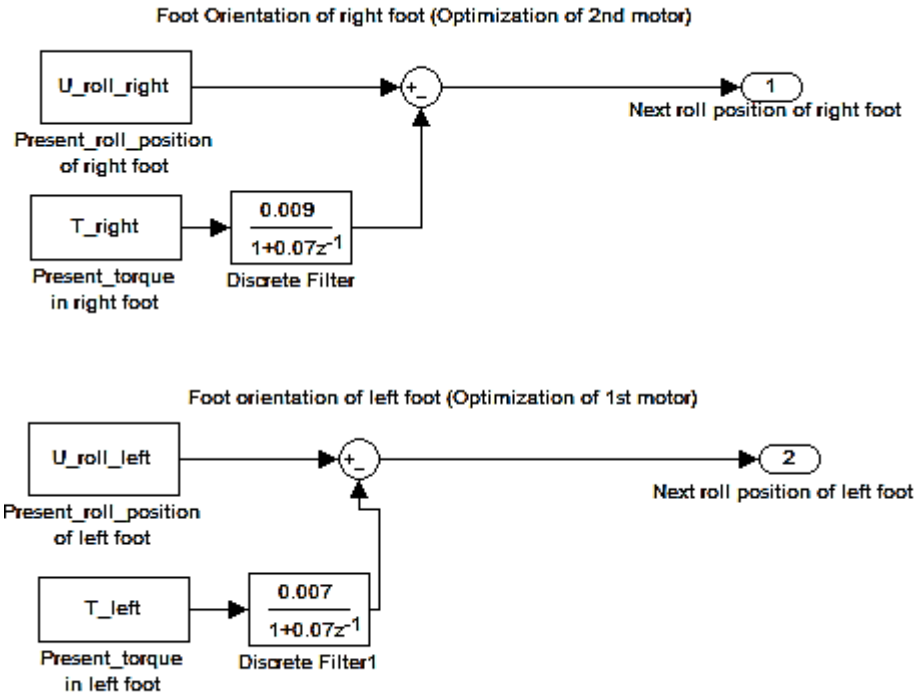

Figure 7.1 Matlab Simulink filters of roll position.

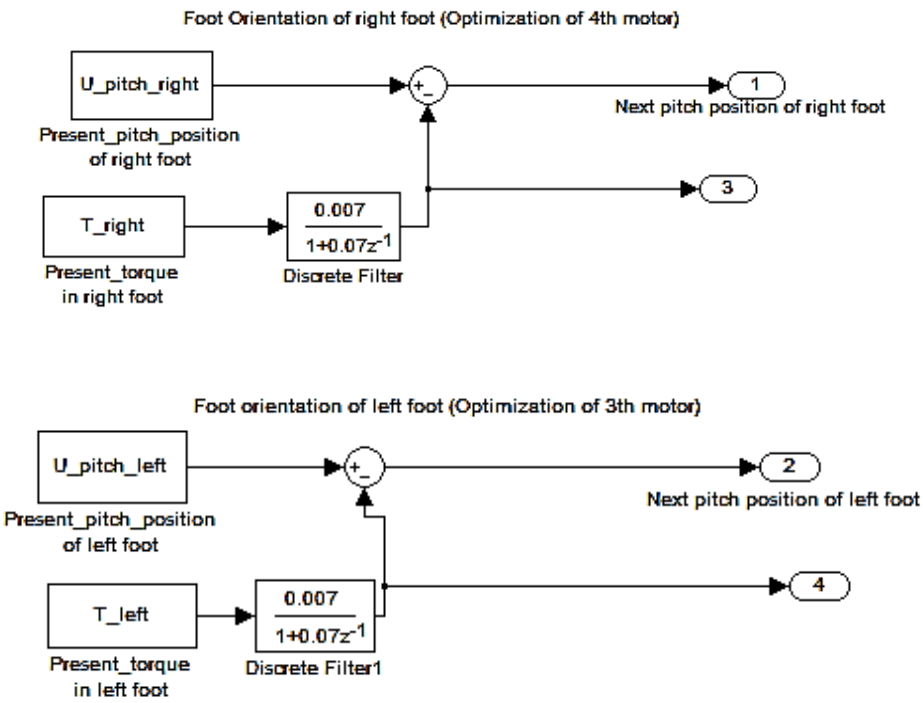

Figure 7.2 Matlab Simulink filters of pitch position.

Figure 7.3 and 7.4 show the foot orientation experiments snapshots.

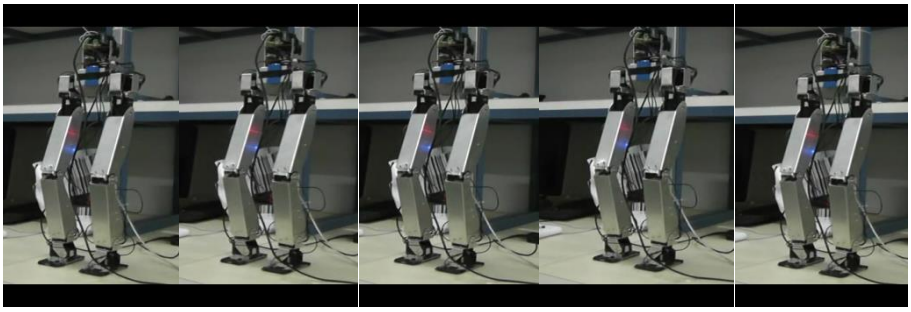

Figure 7.3 The foot orientation experiment snapshots of biped robot.

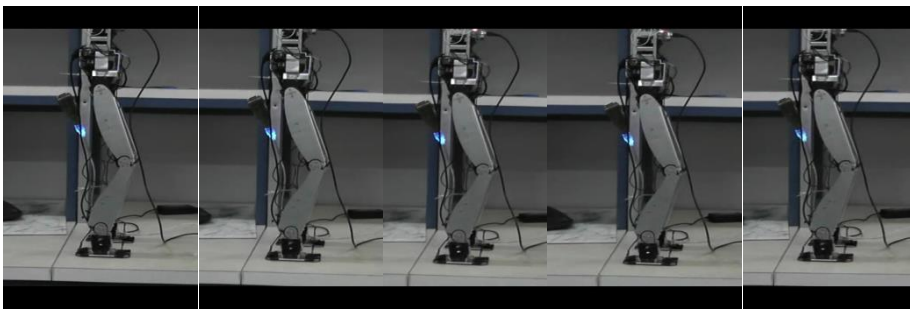

Figure 7.4 The foot orientation experiment snapshots at the sagittal plane.

Figure 7.5 shows the force disturbances and roll-pitch optimizations at the force orientation experiment.

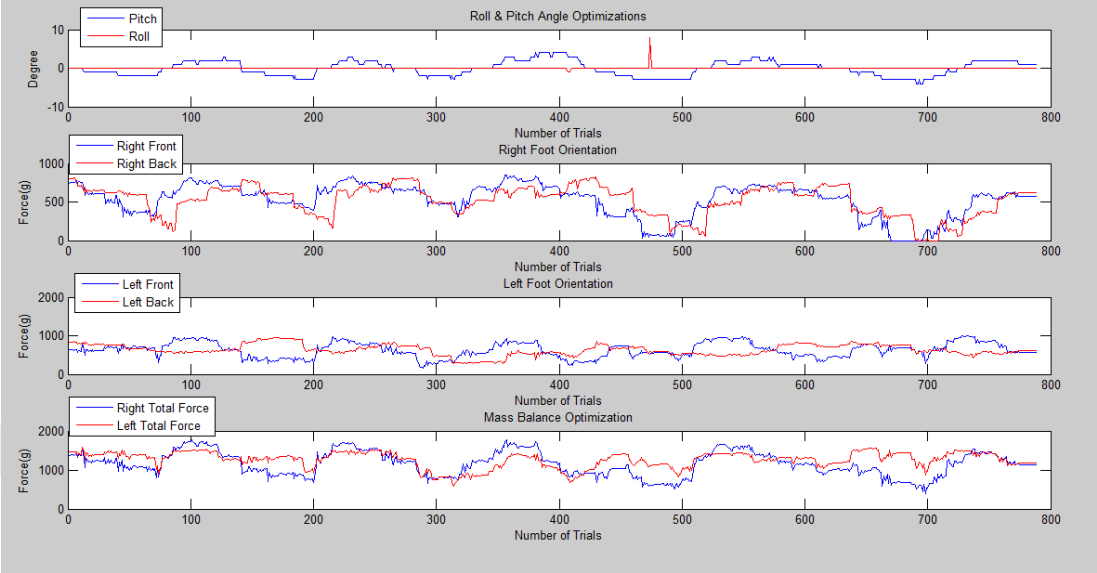

Figure 7.5 The force disturbances and roll-pitch optimizations at the force orientation experiment.

7.2 Trunk Orientation Experiments

Trunk orientation control keeps the robot trunk upright of the ground at walking preparation phase. In this experiment, pitch and roll angles data acquired from the inertial measurement units are processed by filter. Filter process the angles and gives the related joint a correction. Figure 7.6 show the trunk orientation experiments snapshots.

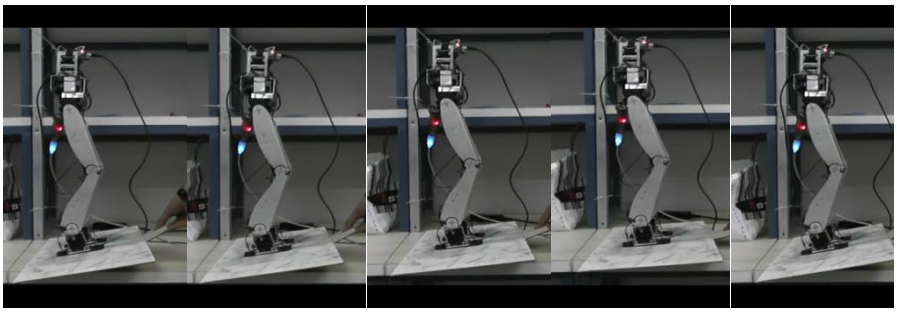

Figure 7.6 The trunk orientation experiment snapshots of biped robot.

MATLAB Simulink filters of pitch position at the sagittal plane are shown in Figure 7.7.

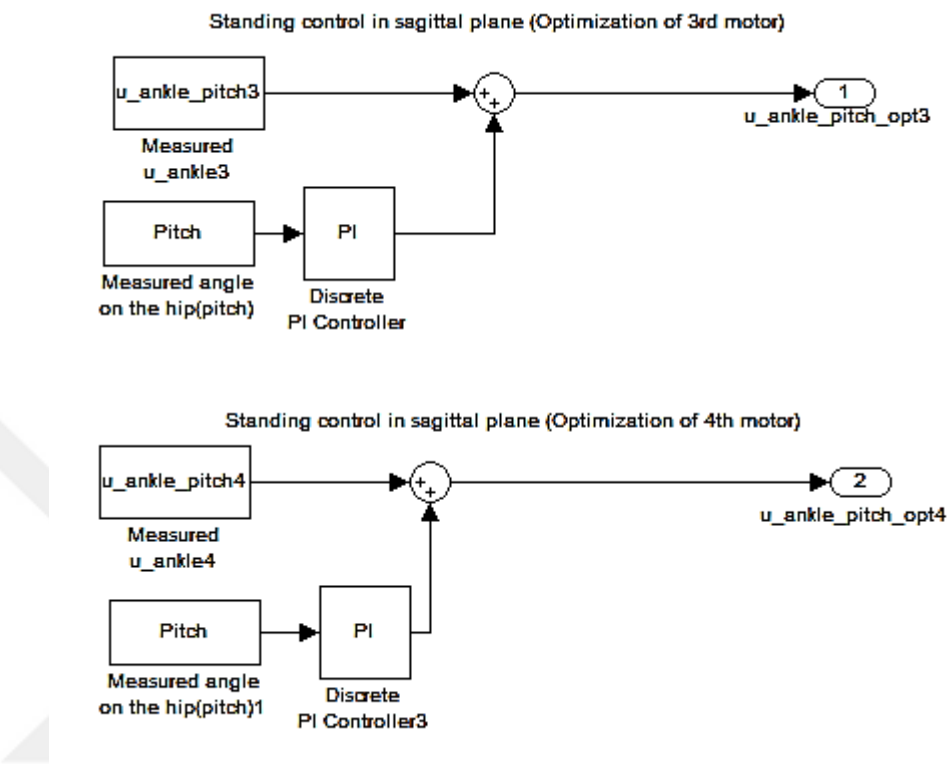

Figure 7.7 Matlab Simulink filters of pitch position at the sagittal plane.

Filters of roll position at the frontal plane are shown in Figure 7.8.

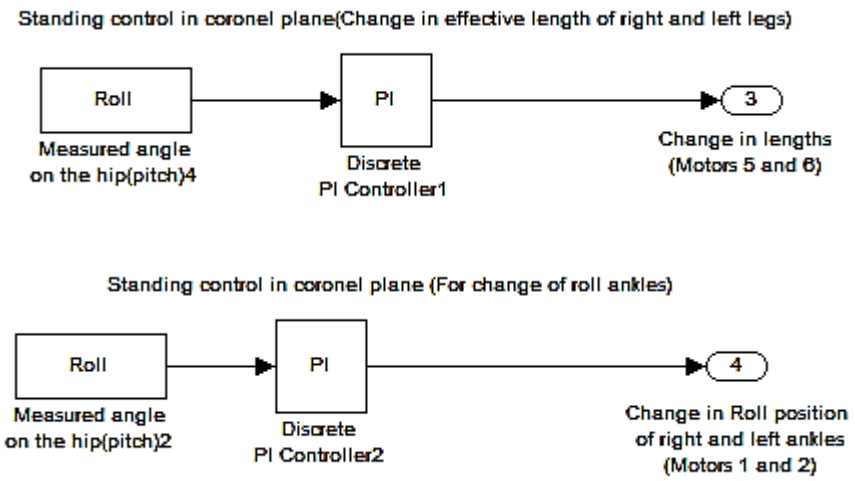

Figure 7.8 Matlab Simulink filters of pitch position at the frontal plane.

7.3 Experimental Determination of CoP

CoP control basis are explained in Section 5.2.2. To analyze the change of CoP during the walking, 8 step walking test was done. Figure 7.9 and 7.10 show CoP change on the foot during the walking.

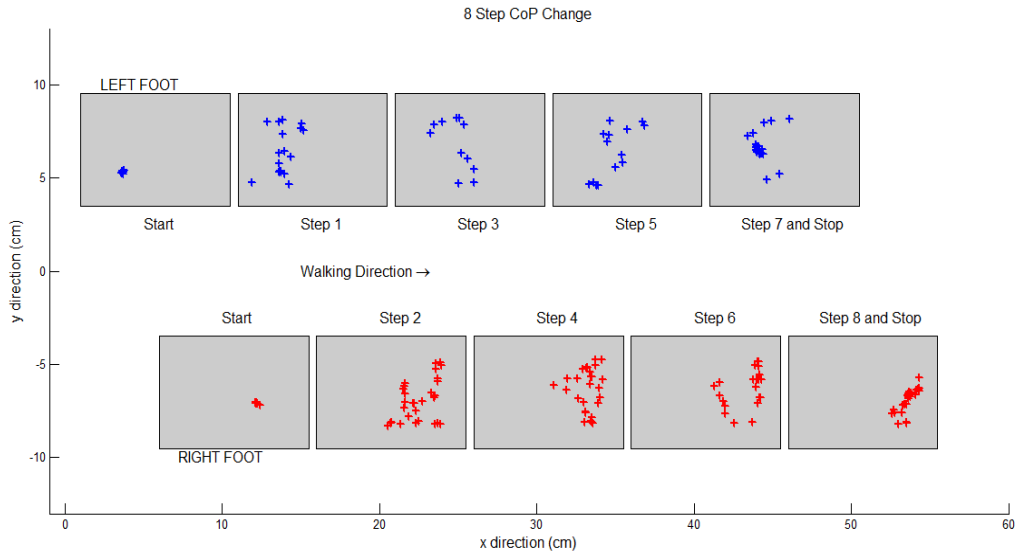

Figure 7.9 CoP change on the foot during the walking (experiment 1).

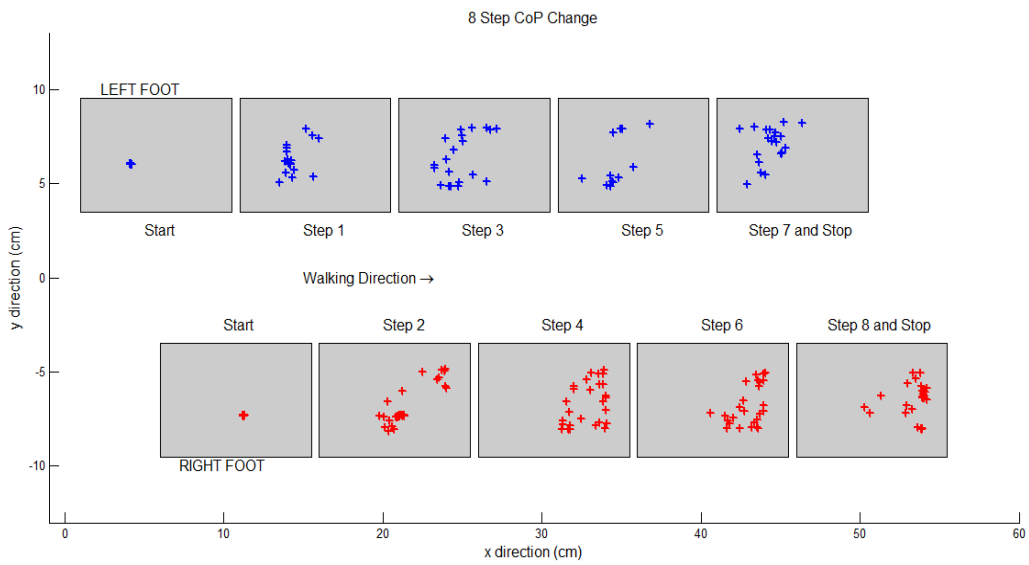

Figure 7.10 CoP change on the foot during the walking (experiment 2).

Figure 7.11 and 7.12 show the force sensors change at the foot during the walking.

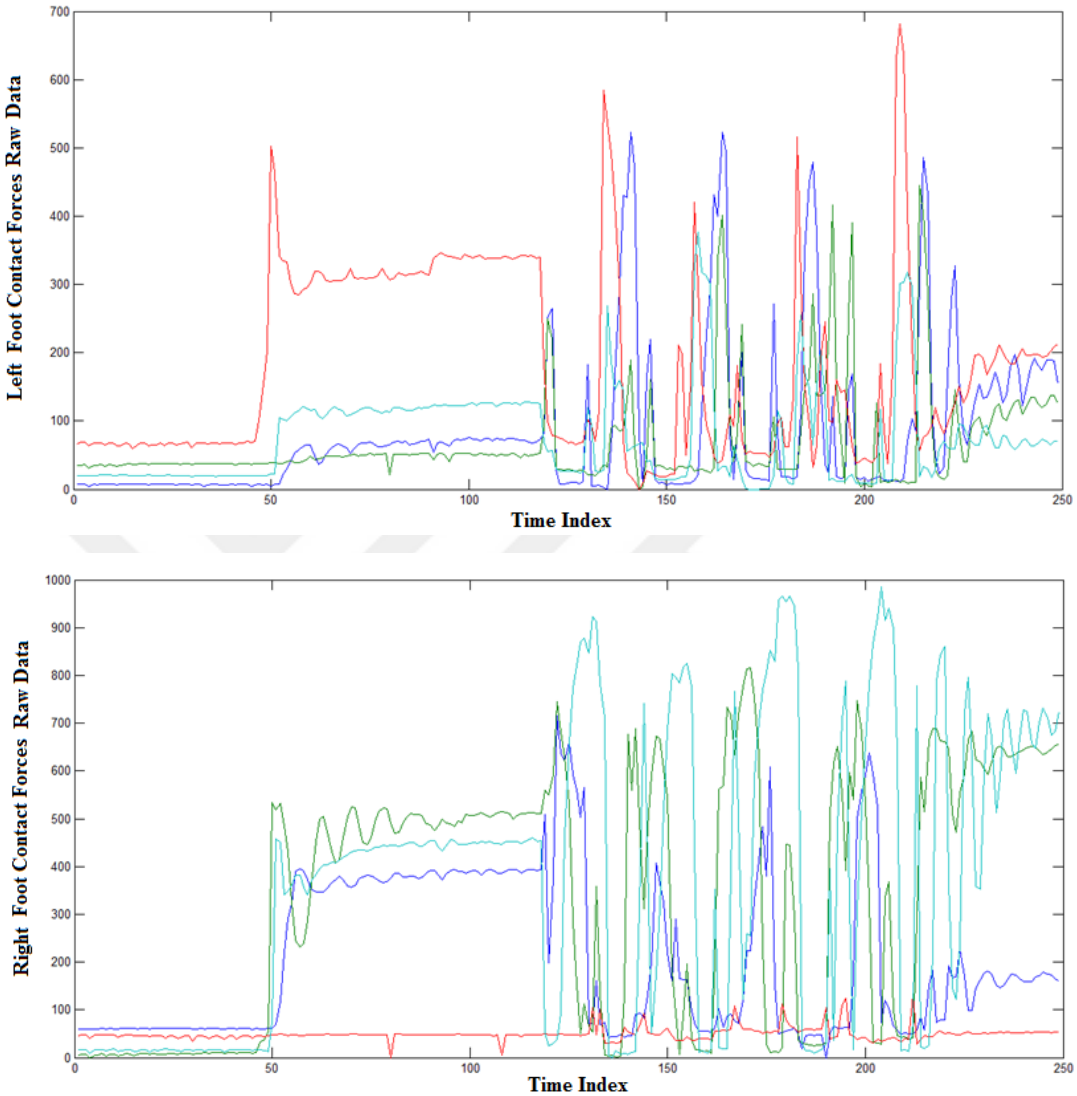

Figure 7.11 The force sensors raw data results at the foot during the walking (experiment 1).

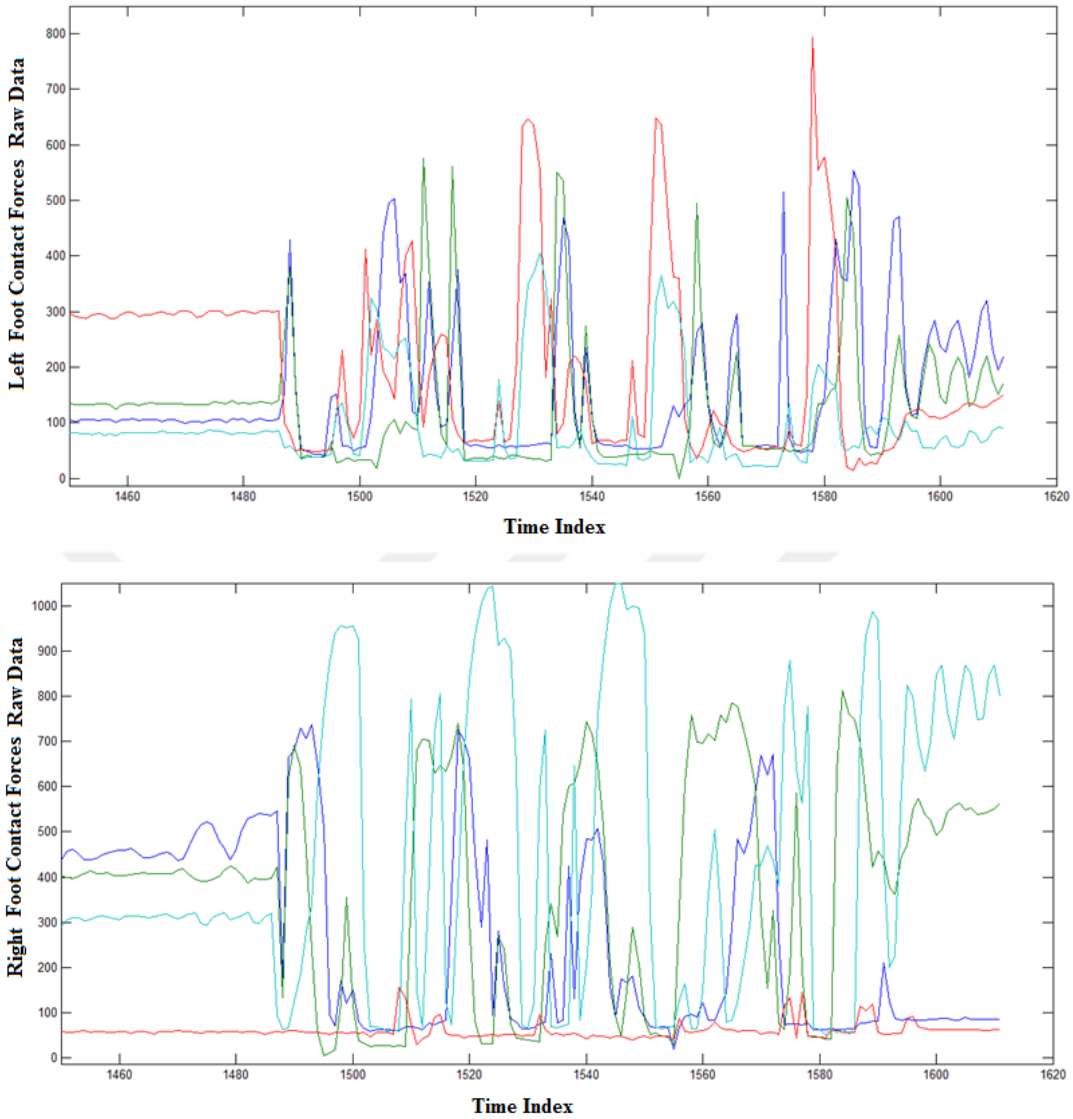

Figure 7.12 The force sensors raw data results at the foot during the walking (experiment 2).

7.4 Walking Experiments

8 step walking test was done by the main walking trajectory. The trunk roll and pitch angles were measured in the walking period. The robot trunk angles without any control except for motor own PI control, are shown in Figure 7.13.

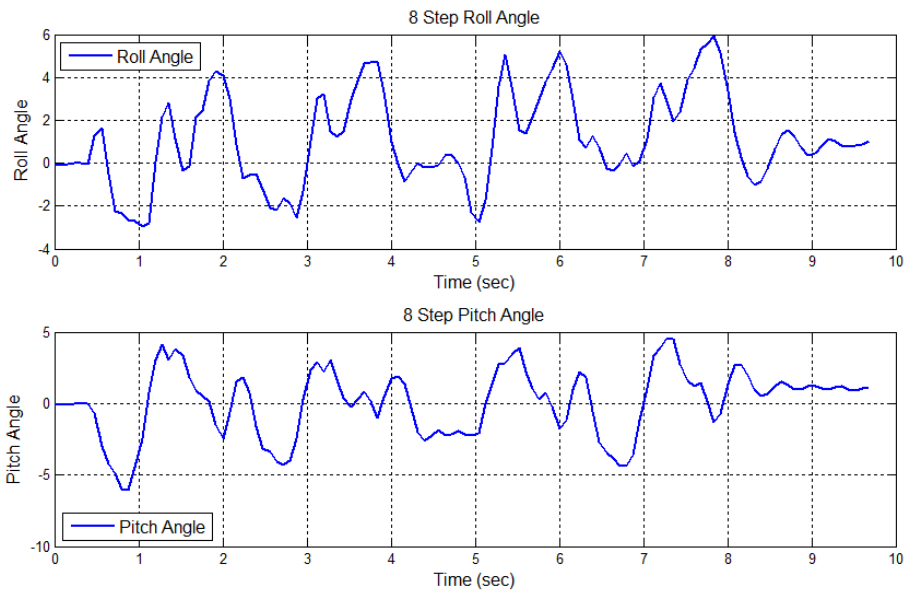

Figure 7.13 The robot trunk angles without any control except for motor own PI control.

It is seen that there are some irregularities of angle changes. Hence, robot continues to walk steadily. Figure 7.14 is shows the robot trunk angles when all controllers open.

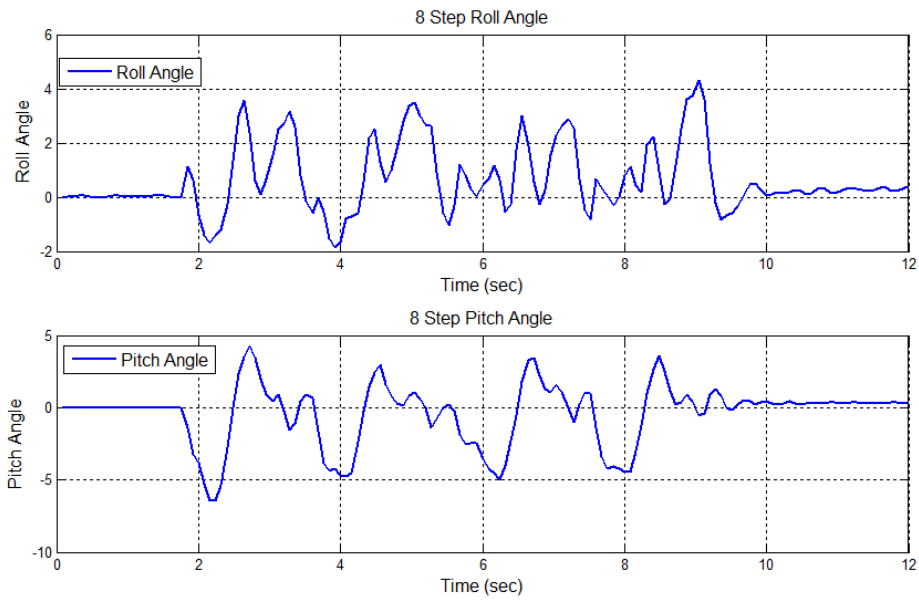

Figure 7.14 The robot trunk angles when all controllers open.

As shown in Figure 13 and 7.14, the trunk angles change range from -6, 6 degrees increases the range -4, 4 degrees when the controllers are activated. Therefore, more

stable walking is obtained with using controls. The robot trunk angles change comparison when all controllers close and open is shown in Figure 7.15.

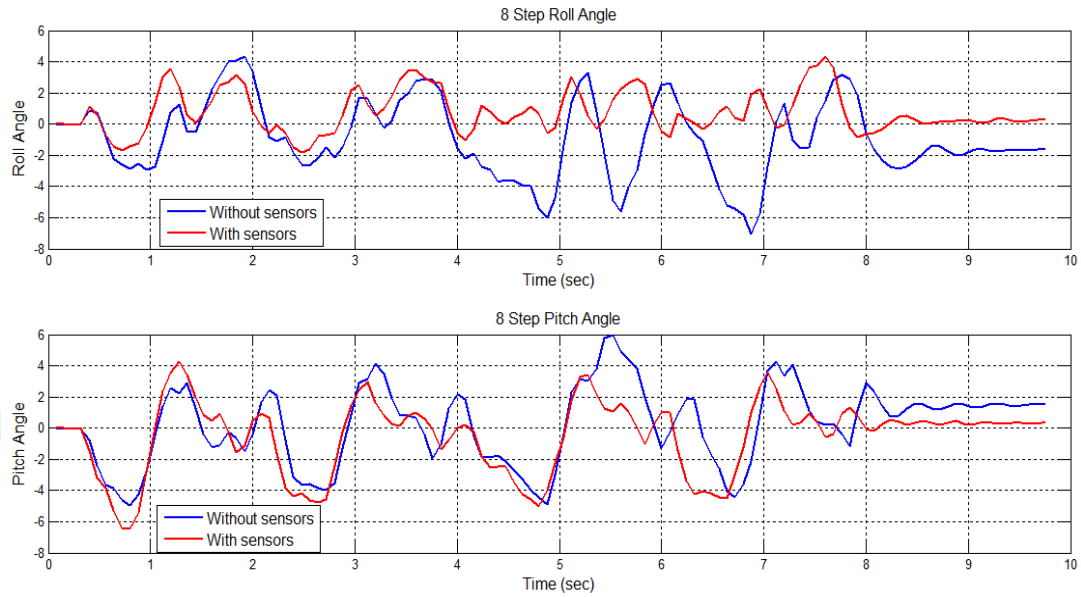

Figure 7.15 The robot trunk angles change comparison when all controllers close and open.

CHAPTER EIGHT
CONCLUSIONS AND FUTURE WORKS

In this thesis, a second generation small biped RUBI-2 is developed for further dynamic robot studies given below by the help of previous experiences on a biped robot AHTO.

The robot RUBI-2 has a human-like locomotion inspired from human leg sizes and leg-foot ratio. Unlike the most of the other similar robot platforms, that robotic structure is designed for smaller foot size and longer leg length, which causes walking and balancing more difficult and challenging. But, this locomotion detail brings more human-like operations for both balancing and walking.

Robot platform of RUBI-2 is composed of several components including mechanical structure, walking pattern generation and actuator angle calculations, sensors and instrumentation, and control algorithms for stable walking and balance operations.

12 DOF biped robot prototype RUBI-2 with a trunk and two legs has been designed and implemented. It is the third version of the biped robot that has been built so far. The requirements of robot like motor-gear combinations are defined by the help of previous studies. The robot is designed using computer aided design software, SolidWorks. The main structure is built with aluminum plates and actuated with smart robot servos.

Platform of RUBI-2 is a modular robot, each part of the robot can be arranged for different purposes such as ground force enhancement under the foot, different types of trunk design, different battery type and placement opportunities, body and arms additions, and etc. Also, different possible embedded controllers may be applied and extra sensory options can be implemented depending on the target areas. Those modularity options make RUBI-2 a general purpose small robot platform for walking

robot studies. This type of small and lightweight robot may be an appropriate platform for beginner researchers in academic and/or commercial developers.

In this study, two well-known humanoid biped robot gait generation methods are analyzed for obtaining biped walking patterns. First, foot parameters method is studied by using cubic spline interpolation. Second, LIPM is studied by using Fourier series approximation. After the generation of the walking pattern, ankle, knee, and hip angles are calculated by the inverse kinematics method. For this purpose, motion simulation software Cosmomotion is used to obtain the actuators' joint angles with walking simulations. Various walking patterns are created, simulated and experimentally tested with different walking parameters. As a result of these studies, an appropriate main walking pattern is created for forward walking by LIPM. Walking patterns are generated offline and stored in a database.

The generated walking patterns can be successfully performed on the robot without any disturbances in an open-loop manner. But in practice, the robot balance is affected by environmental conditions such as inclined floor and instantaneous unexpected causes, thus, each robot should have a control system which is implemented as a compensator for disturbances in order to maintain stability by the help of the sensor devices.

Our robot control system is performed by using force sensors and inertial measurement unit data. Simple mathematical models are used for controllers on the robot. Controllers are improved and tuned through experiments, and robot control strategy is planned for RUBI-2.

The implemented control system is composed of Trunk Orientation Control and Trunk Angle Adjustment based on Inertial Measurement Data, Foot Orientation Control, Early Landing Modification, Impact Compensation and CoP Control based on foot force sensor data. Trunk Orientation Control and Foot Orientation Control are performed only at the initialization of the walk. The rest of the control operations are ready to compensate disturbances in case of detection in a control loop.

The robot RUBI-2 can walk on flat surfaces that contain small uneven areas. Disturbing roll and pitch movements and inclinations of the floor can be detected and compensated successfully by the related controllers. Also, foot contact problems, which may cause balance loss, are treated in a region of control.

Overall, this design and implementation study enables the researcher in-depth understanding of dynamics and control of biped robot. So, this robot can be used as small, lightweight and modular educational and research platform for biped mechanisms.

As a future work, a more and more stable walk of the robot will be developed by the help of the actual model of the robot. At this stage, all control strategies are local solutions for each disturbing event. Although all of the control options are efficient for flat floor walk, further implementations of the robot such as turning, jumping and climbing upstairs require more complex control algorithms. In order to develop more complex control schemes, it is needed to determine a more realistic robot model by using system identification approach. For that purpose, several experiments should be conducted to reach the most realistic model.

Instead of discrete local control, global control can be a solution for developing a human-like walk. The correct theoretical background and efficient model of the robot are required for that purpose.

At the same time, the mechanical structure is inspected for better stability because the actual robotic system has some issues on mechanical coupling. Also, electrical connections and data acquisition should be revised. Several new sensors like small and accurate toque sensor should be added to control algorithm. Maybe, a camera system can be used to get visual environment data.

The robot RUBI-2 has no body parts or arms now. In the future, the robot may be transformed into a more humanoid type with the addition of the rest of the human-like body components. At that time, a more human-like operation may occur.

The robot is walking now by the help of a personal computer connection. As parallel, an embedded computer structure is implemented. By the application of that embedded mini computer system with a wireless connection, a more efficient and autonomous walk is expected. Now, the weight addition from that embedded system is not taken into account for the balance algorithm.

REFERENCES

Capek, K. (1923). *R.U.R. Rossum's Universal Robots*. New York: Dover Publications.

Ching-Long, S. (1999). Ascending and descending stairs for a biped robot. *IEEE Transactions on Systems, Man, and Cybernetics - Part A: Systems and Humans, 29*(3), 255-268.

Erbatur, K., & Kurt, O. (2009). Natural ZMP trajectories for biped robot reference generation. *IEEE Transactions on Industrial Electronics, 56*(3), 835-845.

Fujimoto, Y., & Kawamura, A. (1998). Simulation of an autonomous biped walking robot including environmental force interaction. *IEEE Robotics & Automation Magazine, 5*(2), 33-42.

Golliday, C., & Hemami, H. (1977). An approach to analyzing biped locomotion dynamics and designing robot locomotion controls. *IEEE Transactions on Automatic Control, 22*(6), 963-972.

Goswami, A. (1999). Foot rotation indicator (FRI) point: a new gait planning tool to evaluate postural stability of biped robots. Paper presented at the *Robotics and Automation, 1999. Proceedings. 1999 IEEE International Conference, 41, 1*, 47-52.

Goswami, A. (1999). Postural stability of biped robots and the foot-rotation indicator (FRI) point. *The International Journal of Robotics Research, 18*(6), 523-533.

Hemami, H., Weimer, F., & Koozekanani, S. (1973). Some aspects of the inverted pendulum problem for modeling of locomotion systems. *IEEE Transactions on Automatic Control, 18*(6), 658-661.

Hirai, K., Hirose, M., Haikawa, Y., & Takenaka, T. (1998). The development of Honda humanoid robot. Paper presented at the *Robotics and Automation, 1998. Proceedings. 1998 IEEE International Conference, 1322, 2*, 1321-1326.

Inman, V. T., Ralston, H. J., Todd, F., & Lieberman, J. C. (1981). *Human walking*. Baltimore: Williams & Wilkins.

Kajita, S., Kanehiro, F., Kaneko, K., Fujiwara, K., Harada, K., Yokoi, K., & Hirukawa, H. (2003). Biped walking pattern generation by using preview control of zero-moment point. Paper presented at the *Robotics and Automation, 2003. Proceedings. ICRA '03. IEEE International Conference, 1622, 2*, 1620-1626.

Kaneko, K., Kanehiro, F., Morisawa, M., Akachi, K., Miyamori, G., Hayashi, A., & Kanehira, N. (2011). Humanoid robot HRP-4 - Humanoid robotics platform with lightweight and slim body. Paper presented at the *2011 IEEE/RSJ International Conference on Intelligent Robots and Systems*, 4400-4407.

Kim, J.-H., & Oh, J.-H. (2004). Realization of dynamic walking for the humanoid robot platform KHR-1. *Advanced Robotics, 18*(7), 749-768.

Kim, J.-Y., Lee, J., & Ho, J.-H. (2007). Experimental realization of dynamic walking for a human-riding biped robot, HUBO FX-1. *Advanced Robotics, 21*(3-4), 461-484.

Kim, J.-Y., Park, I.-W., & Oh, J.-H. (2006). Experimental realization of dynamic walking of the biped humanoid robot KHR-2 using zero moment point feedback and inertial measurement. *Advanced Robotics, 20*(6), 707-736.

Kim, J.-Y., Park, I.-W., & Oh, J.-H. (2007). Walking Control Algorithm of Biped Humanoid Robot on Uneven and Inclined Floor. *Journal of Intelligent and Robotic Systems, 48*(4), 457-484.

Kun, A. L., & Miller, W. T. (1999). Control of variable speed gaits for a biped robot. *IEEE Robotics & Automation Magazine, 6*(3), 19-29.

McMahon, T. A. (1984). *Muscles, reflexes, and locomotion*. Princeton, NY: Princeton University Press.

Miller, W. T. (1994). Real-time neural network control of a biped walking robot. *IEEE Control Systems, 14*(1), 41-48.

Park, I. W., Kim, J. Y., & Oh, J. H. (2006). Online biped walking pattern generation for humanoid robot KHR-3(KAIST humanoid robot - 3: HUBO). Paper presented at the *2006 6th IEEE-RAS International Conference on Humanoid Robots*, 398-403.

Qiang, H., Nakamura, Y., Arai, H., & Tanie, K. (2000). Development of a biped humanoid simulator. Paper presented at the *Intelligent Robots and Systems, 2000. (IROS 2000). Proceedings. 2000 IEEE/RSJ International Conference, 1933, 3*, 1936-1942.

Qiang, H., Yokoi, K., Kajita, S., Kaneko, K., Arai, H., Koyachi, N., & Tanie, K. (2001). Planning walking patterns for a biped robot. *Robotics and Automation, IEEE Transactions on, 17*(3), 280-289.

Reilly, K. (2011). From automata to automation: The birth of the robot in R.U.R. (Rossum's universal robots) *Automata and Mimesis on the Stage of Theatre History* (pp. 148-176). London: Palgrave Macmillan UK.

Vukobratovic, M., & Borovac, B. (2004). Zero-moment point — Thirty five years of its life. *International Journal of Humanoid Robotics, 01*(01), 157-173.

Youngjin, C., Bum-Jae, Y., & Sang-Rok, O. (2004). On the stability of indirect ZMP controller for biped robot systems. Paper presented at the *Intelligent Robots and Systems, 2004. (IROS 2004). Proceedings. 2004 IEEE/RSJ International Conference*, 1962, *2*, 1966-1971.

Yu, O., Aikawa, H., Shimomura, K., Kondo, H., Morishima, A., Hun-ok, L., & Takanishi, A. (2006). Development of a new humanoid robot WABIAN-2. Paper presented at the *Proceedings 2006 IEEE International Conference on Robotics and Automation, 2006. ICRA 2006*, 76-81.

Zhe, T., Changjiu, Z., & Zenqi, S. (2003). Trajectory planning for smooth transition of a biped robot. Paper presented at the *Robotics and Automation, 2003. Proceedings. ICRA '03. IEEE International Conference, 2452, 2*, 2455-2460.